JACS
JOURNAL OF THE AMERICAN CHEMICAL SOCIETY

Perspective

pubs.acs.org/JACS

Recent Advances in the Synthesis and Functions of Reconfigurable Interlocked DNA Nanostructures

Chun-Hua Lu, Alessandro Cecconello, and Itamar Willner*

The Institute of Chemistry, The Hebrew University of Jerusalem, Jerusalem 91904, Israel

ABSTRACT: Interlocked circular DNA nanostructures, e.g., catenanes or rotaxanes, provide functional materials within the area of DNA nanotechnology. Specifically, the triggered reversible reconfiguration of the catenane or rotaxane structures provides a means to yield new DNA switches and to use them as dynamic scaffolds for controlling chemical functions and positioning functional cargoes. The synthesis of two-ring catenanes and their switchable reconfiguration by pH, metal ions, or fuel/anti-fuel stimuli are presented, and the functions of these systems, as pendulum or rotor devices or as switchable catalysts, are described. Also, the synthesis of three-, five-, and seven-ring catenanes is presented, and their switchable reconfiguration using fuel/anti-fuel strands is addressed. Implementation of the dynamically reconfigured catenane structures for the programmed organization of Au nanoparticle (NP) assemblies, which allows the plasmonic control of the fluorescence properties of Au NP/fluorophore loads associated with the scaffold, and for the operation of logic gates is discussed. Interlocked DNA rotaxanes and their different synthetic approaches are presented, and their switchable reconfiguration by means of fuel/anti-fuel strands or photonic stimuli is described. Specifically, the use of the rotaxane as a scaffold to organize Au NP assemblies, and the control of the fluorescence properties with Au NP/fluorophore hybrids loaded on the rotaxane scaffold, are introduced. The future prospectives and challenges in the field of interlocked DNA nanostructures and the possible applications are discussed.

1. INTRODUCTION

The base sequence encoded in nucleic acids provides structural and functional information within the biopolymers,[1] Figure 1. The stabilities of different oligonucleotide structures are controlled by the nucleotide base sequence comprising the biopolymers[2] and by environmental parameters affecting the nucleotides or their supramolecular self-assembly properties. Different parameters control the stabilities of nucleic acid structures, such as number of base pairs, nature of the bases, ionic strength, pH, cooperative binding of metal ions, supramolecular ion-assisted assembly of G-quadruplexes, cooperative binding of intercalators or photoisomerizable units, and more. The transition from one DNA structure to another structure requires an input trigger that drives an energetically downhill process (ΔG), and switchable reversibility is achieved by applying counter triggers. For example, Figure 1A presents the input-triggered strand displacement of a toehold-functionalized duplex nucleic acid **I**, composed of nucleic acids **1**/**2**, by an input strand **3** that includes a counter toehold $\mathbf{a_t}$*.[3] As the input strand includes domain $\mathbf{a_t}$*, complementary to the toehold domain $\mathbf{a_t}$ of complex **I**, hybridization of the input to the complex starts branch migration and the displacement of strand **2**, with the concomitant formation of the energetically stabilized duplex **1**/**3**, structure **II**. Figure 1B,C depicts a series of switchable

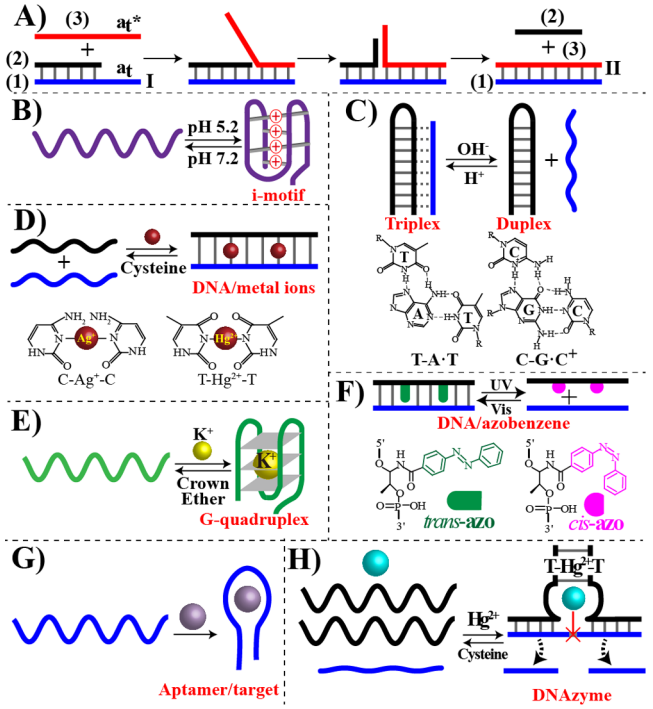

Figure 1. Examples for the structural and functional information encoded in oligonucleotides. (A) Duplex formation and strand displacement of duplex oligonucleotide structures. (B) pH-stimulated transitions between i-motif and single-strand structures. (C) pH-stimulated triplex-to-duplex transitions using C-G·C$^+$ and T-A·T as triplex motives. (D) Switchable metal-ion/ligand bridging and dissociation of duplex DNAs using T-Hg^{2+}-T or C-Ag$^+$-C bridges and their cysteine-mediated dissociation. (E) Switchable K$^+$-ion/crown ether transitions between a G-quadruplex and single-strand states. (F) Light-induced switchable transitions between a duplex structure and single strands using a photoisomerizable azobenzene intercalator. (G) Formation of an energetically stabilized aptamer−ligand complex. (H) Metal-ion/ligand-stimulated activation and deactivation of the hydrolytic DNAzyme.

Received: January 20, 2016
Published: March 28, 2016

DOI: 10.1021/jacs.6b00694
J. Am. Chem. Soc. 2016, 138, 5172−5185

input-triggered transitions of oligonucleotide structures. Figure 1B depicts the pH-induced formation of the cytosine-rich i-motif structure at an acidic pH, and regeneration of the random coiled structure at neutral pH.[4] Figure 1C shows the pH-stimulated duplex-to-triplex transition of DNA structures through the stabilization of C−G·C$^+$-bridged triplexes at an acidic pH,[5] or T−A·T-bridged triplexes at neutral pH.[6] Figure 1D shows the metal-ion-assisted formation of duplex oligonucleotide structures stabilized by cooperative C-Ag$^+$-C[7] or T-Hg^{2+}-T[8] bridges and the separation of the complex by the elimination of the metal ions by the appropriate ligand, e.g., cysteine. Figure 1E shows the rearrangement of a guanosine-rich DNA sequence into the K$^+$-stabilized G-quadruplex supramolecular complex[9] and the reversed formation of the random-coil single strand in the presence of 18-crown-6-ether, which binds and eliminates the stabilizing K$^+$ ions. Figure 1F highlights the photochemical control of DNA structures[10] by *trans*-azobenzene units, tethered to the oligonucleotide strand, that stabilize cooperatively the duplex structures via intercalation into the double-stranded assembly. In turn, photoisomerization of *trans*-azobenzene to *cis*-azobenzene yields a photoisomer lacking affinity to the duplex DNA, thus leading to the separation of the duplex.

Functional properties encoded in the base sequence of DNA include specific recognition properties toward low-molecular-weight substrates, or macromolecules (aptamers),[11] and sequence-dictated catalytic functions (DNAzymes or ribozymes).[12] For example, Figure 1G depicts the formation of the aptamer−substrate complex in the presence of the appropriate target. Similarly, the cooperative stabilization of a non-catalytically active DNAzyme into a catalytically active DNAzyme structure via metal-ion-stimulated formation of duplex bridges,[13] and the ligand-induced separation of the supramolecular DNAzyme assembly, are presented in Figure 1H.

Different sequence-dictated switchable reconfigurations of DNA structures and control of DNA functions have been extensively used to develop DNA switches,[10,14] DNA logic gates[15] and computing circuits,[16] reconfigurable DNA structures,[17] DNA machines,[18] and catalytic DNAzyme cascades.[19] Interlocked DNA rings composed of catenanes, knots, and Borromean rings appear in nature,[20] and synthetic methodologies to synthesize man-made duplicates have been reported.[21] By the encoding of appropriate base sequence information into the interlocked DNA structures, reconfigurable and stimuli-triggered reconfiguration of the interlocked DNA structures may be envisaged. The present Perspective summarizes recent advances in the synthesis and stimuli-triggered reconfiguration of interlocked DNA catenanes and rotaxane systems. Specifically, emerging functions resulting upon reconfiguring the interlocked DNA scaffolds, such as switchable catalysis, switchable plasmonic properties, and programmed organization of nanoparticles, are discussed.

2. TWO-RING INTERLOCKED CATENANE NANOSTRUCTURES

The synthesis of two-ring interlocked catenanes may be accomplished by several paths that follow several basic common principles. One method, Figure 2A, includes a duplex DNA where the 3′- and 5′-ends comprising the duplex are elongated by single-strand tethers **x,y** and **z,w**. Capping of the domains **x,y** and **z,w** with appropriate caps, followed by ligation of the 3′- and 5′-ends of the units, leads then to the formation

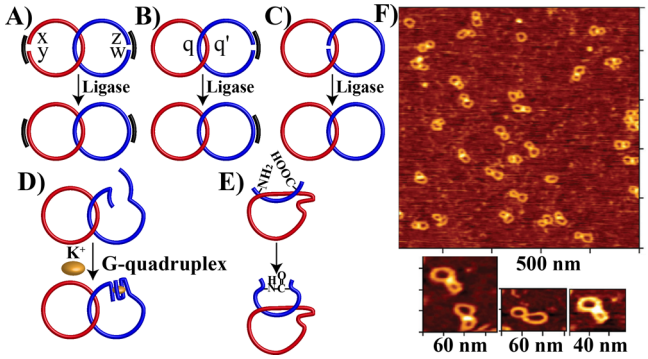

Figure 2. Schematic assembly of interlocked two-ring DNA catenanes: (A) by the enzymatic ligation of two inter-threaded strands, (B) by the enzymatic ligation of a single-strand threaded into a circular DNA, (C) by the enzymatic ligation of a threaded single strand into a circular DNA, stabilized by cooperative base-pairing with the circular DNA at the ligation site, (D) by the inter-threading of a single-strand oligonucleotide into a circular DNA and the formation of a supramolecular lock by oligonucleotide functionalities at the 3′- and 5′-ends of the threaded strand, e.g., a K$^+$-ion-stabilized G-quadruplex, and (E) by the covalent linkage (e.g., amide bond) of chemical functionalities associated with the 3′- and 5′-ends of a strand threaded into a circular DNA. (F) AFM image corresponding to double-stranded two-ring interlocked circular DNA catenanes. Large image recorded in intermittent contact mode (top), and higher magnification images recorded in tapping mode in liquid (bottom). Reproduced with permission from ref 27. Copyright 2014 The Royal Society of Chemistry.

of the interlocked catenane structure.[22] A second method,[22,23] Figure 2B, involves the primary synthesis of a single DNA ring and the inter-threading of a single-stranded nucleic acid that is complementary to a domain of the DNA ring scaffold (domains **q**/**q**′). Capping of the single-strand ends might proceed on the single-stranded domain of the inter-threaded nucleic acid, Figure 2B,[23] or by ligation on the complementary domain linking the two strands in the absence of an auxiliary strand, Figure 2C.[22] A further approach involves locking the inter-threaded single strand in the DNA ring scaffold by supramolecular complexes or covalent bonds. For example, the design of G-rich domains at the 3′- and 5′-ends of the inter-threaded strand, in the presence of K$^+$-ions, results in a G-quadruplex structure that locks the two strands into a [2]catenane structure,[24] Figure 2D. Alternatively, the DNA ring-inter-threaded strand was functionalized with amine/carboxylic acid functionalities, and the coupling led to the locking of the rings by a covalent amide bond,[25] Figure 2E. Often, the single-strand inter-threaded DNA scaffolds are rigidified by the addition of complementary nucleic acid sequences that render the circular structures of the interlocked catenanes stiffer.[26,27] The different methods to assemble the catenated structures require the purification of the interlocked systems from supramolecular structures exhibiting kissing interaction and/or unreacted strands. Typically, purification is accomplished by HPLC or electrophoretic separation, and the products are characterized by mass spectrometry and AFM imaging. The yields of the catenated nanostructures are usually in the range of 10−40%. For example, Figure 2F depicts AFM images of two-ring catenane nanostructures, where the rings were rigidified by duplex domains.[27]

The base sequences encoded in the catenanes provide means to reversibly switch the interlocked two-circle structures. For

DOI: 10.1021/jacs.6b00694
J. Am. Chem. Soc. 2016, 138, 5172−5185

example, the two-ring catenane **M**, which includes the complementary inter-ring domain **a**/**a**′ and rigidified circular domains, was treated with the fuel strand **4**, which separated the **a**/**a**′ inter-circle domain to yield the "open" two-circle catenane **N**, Figure 3A.[27] Treatment of the resulting structure with the anti-fuel strand **5** removed the fuel-strand **4** by forming the energetically stabilized "closed" catenane **M**. By labeling the rigidifying strands with a fluorophore (Cy3) and a quencher (BHQ-2), the dynamic cyclic transitions of the catenane between the "closed" (**M**) and "open" (**N**) catenane states were then probed by the fluorescence intensities of the fluorophore label, Figure 3B.

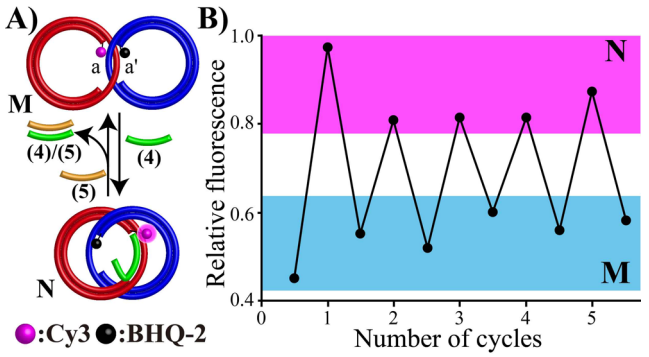

Figure 3. (A) Switchable reconfiguration of a double-stranded two-ring interlocked catenane between a hybridized junction, state **M**, and a dissociated interlocked structure, state **N**, using fuel and anti-fuel strands. The reconfiguration is followed by probing the catenane using a fluorophore/quencher pair. (B) Cyclic fluorescence changes upon the fuel/anti-fuel-stimulated reconfiguration of the system between state **M** (low fluorescence) and state **N** (high fluorescence). Adapted with permission from ref 27. Copyright 2014 The Royal Society of Chemistry.

A three-station DNA catenane rotary motor exhibiting directional operation was obtained by encoding into the catenane structure specific binding domains that are occupied by appropriate external triggers, Figure 4A.[28] In the two-ring DNA catenane α/β, ring β provides the rotation track for ring α, and it includes three binding domains for hybridization with ring α. In state **A** of the rotor, ring α rests on one binding domain, **a**, of ring β, through complementary base-pair hybridization. The binding domain **b** is partially blocked by the C-rich sequence **6**, and binding domain **c** includes partial complementarity with two base mismatches with respect to ring α. Under these conditions, ring α is confined to the domain **a**, which yields the energetically favored duplex structure. Subjecting the system to pH = 5.2 separates strand **6** from ring β through the formation of the i-motif structure. The release of **6** from ring β leads to the vacant binding domain **b**, which yields a duplex structure with ring α exhibiting enhanced stability as compared to the original hybridization with domain **a**. This results in the rotation of ring α from state **A** to state **B**. Subsequent neutralization of the system to pH = 7.2 and its interaction with Hg^{2+} result in the T-Hg^{2+}-T cooperatively stabilized duplex between ring α and domain **c** of ring β, leading to the transition of ring α from state **B** to state **C**. Subsequent treatment of state **C** with cysteine removed the Hg^{2+} ions from the duplex in domain **c**, and the weakened duplex in state **C** led to the transition of ring α to domain **a**, which yields the energetically stabilized duplex, state **A**. The reverse treatment of state **A** with Hg^{2+} at pH = 7.2 dictated the

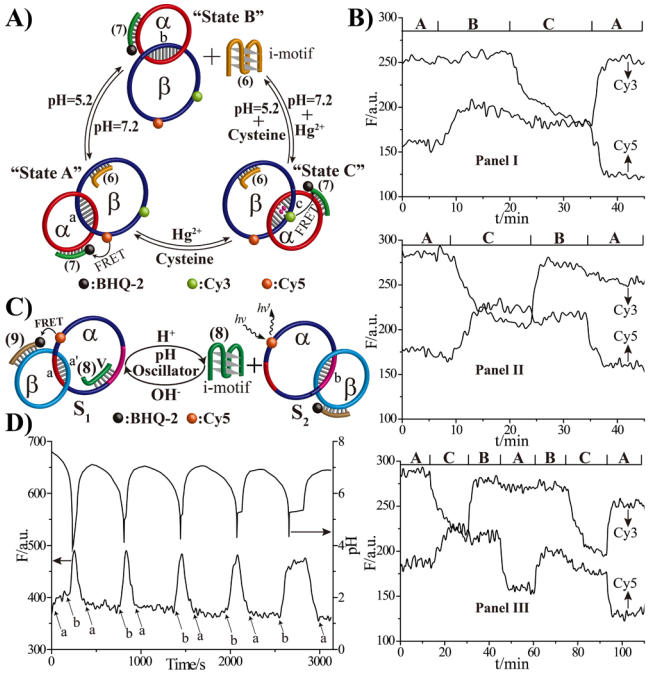

Figure 4. (A) Schematic operation of an interlocked catenane rotary motor exhibiting controlled directionality using Hg^{2+}/cysteine and pH (5.2/7.2) as triggers and anti-triggers for the activation of the rotor. The rotation is probed by labeling of ring β with two fluorophores (Cy3 and Cy5) and ring α functionalized with a quencher-modified strand. (B) Time-dependent fluorescence changes upon the triggered activation of the rotor. Panel I: Clockwise rotation across states A→B→C→A. Panel II: Counter-clockwise rotation across states A→C→B→A. Panel III: Counter-clockwise rotation of the system across states A→C→B→A followed by a clockwise rotation cycle across states A→B→C→A. Adapted with permission from ref 28. Copyright 2013 American Chemical Society. (C) A pH-triggered two-ring catenane "pendulum". (D) Time-dependent fluorescence changes and respective pH oscillations, upon the triggered operation of the "DNA pendulum". Adapted with permission from ref 30. Copyright 2013 American Chemical Society.

transformation of ring α from state **A** to state **C**, whereas the interaction of state **C** with cysteine at pH = 5.2 restored state **B**. Similarly, subjecting state **B** to pH = 7.2 dissociated the separated i-motif structure as a regenerated state **A**. By the internal labeling of ring β with two fluorophores, Cy3 and Cy5, and by the decoration of the rotating ring α with the BHQ-2-functionalized nucleic acid **7**, the stimuli-controlled rotation of ring α on the track β could be probed by following the fluorescence intensities of the fluorophore labels associated with ring β. In state **A**, the fluorophore Cy5 is effectively quenched, while Cy3 is inefficiently quenched. In state **C**, the fluorophore Cy3 is effectively quenched, while Cy5 is inefficiently quenched. In state **B**, the two fluorophores, Cy3 and Cy5, are spatially separated from the quencher unit, leading to inefficient quenching of the two fluorophores.

Figure 4B depicts the time-dependent fluorescence changes of the two fluorophores upon the sequential clockwise rotary transitions **A**→**B**→**C**→**A**, the counter-clockwise transitions **A**→**C**→**B**→**A**, and the sequential counter-clockwise and clockwise rotation of ring α, **A**→**C**→**B**→**A**→**B**→**C**→**A**, upon applying the respective triggering stimuli on the rotary device. A detailed kinetic analysis of the rotation processes revealed that the stimuli-triggered binding of ring α on ring β follows the selection of the shortest path to occupy a specific binding

DOI: 10.1021/jacs.6b00694
J. Am. Chem. Soc. 2016, 138, 5172−5185

domain. This leads to the stimuli-triggered directional rotation of ring α on the track β (in clockwise or counter-clockwise directions). An analogous DNA catenane rotary motor that implements the strand displacement mechanism and fuel and anti-fuel strands as triggers was reported.[29] The pH-triggered transition of a two-ring catenane system between two states was implemented to develop a DNA catenane "pendulum" in the presence of an oscillatory pH system,[30] Figure 4C. The catenane pendulum system is composed of the two rings, α and β. In state $\mathbf{S_1}$, ring β rests on domain **a** of ring α, through a duplex domain **a**/**a**′ in the catenated rings. Domain **b** in ring α includes a second binding domain for ring β, and part of this domain is blocked by the C-rich sequence **8**. At an acidic pH (pH ≈ 5.0), the sequence **8** reconfigures into the i-motif structure, which dissociates from the catenane system. Release of the blocker strand **8**, then, allows for the transition of ring β to the vacant binding domain **b**, state $\mathbf{S_2}$, which reveals higher binding affinity toward ring β as compared to domain **a**. Neutralization of the system (pH ≈ 7.0) dissociates the i-motif structure, and the resulting strand displaces ring β from domain **b** to yield state $\mathbf{S_1}$, where ring β hybridizes with domain **a**, and domain **b** is partially blocked by **8**. The transitions of the DNA catenane pendulum device between states $\mathbf{S_1}$ and $\mathbf{S_2}$ were followed by time-dependent fluorescence spectroscopy by the internal labeling of ring α with the fluorophore Cy5, and the functionalization of ring β with the BHQ-2 quencher-modified nucleic acid **9**. The intimate distance between the fluorophore and the quencher units in state $\mathbf{S_1}$ leads to effective quenching of the fluorophore's emission, whereas the spatial separation of the fluorophore and quencher units in state $\mathbf{S_2}$ leads to a higher fluorescence intensity of the fluorophore. The DNA–catenane system was inserted into the well-known IO^{3-}, SO_3^{2-}/$Fe(CN)_6^{4-}$ Landolt-type oscillatory pH system, which oscillates the pH of the system between values 5 and 7.[31] The DNA–catenane system responds to the pH oscillations by dynamic switching of the system between states $\mathbf{S_1}$ and $\mathbf{S_2}$, Figure 4D. The pendulum activities of the DNA–catenane were probed by the time-dependent fluorescence changes of the DNA device, and these followed the dynamic oscillatory pH changes of the system.

Triggered re-configuration of the two-ring catenane system was further used to design switchable DNAzyme catalytic systems.[32] Figure 5A depicts the fuel-driven formation/dissociation of the hemin/G-quadruplex complex on a single-strand two-ring catenane scaffold. The catenane consists of two rings, α and β, where ring α includes sequence **I**, which corresponds to the G-quadruplex region. Part of this sequence, **x**, and the additional sequence, **y**, form domain **II**, complementary to the domain **II**′ associated with ring β. The sequence domains **z** and **w** associated with ring α form domain **III** and are blocked by the fuel strand **Fu1**. Under these conditions, "state **A**", formation of the G-quadruplex on ring α is prohibited, due to the partial hybridization of domain **I** by ring β. Displacement of the fuel strand **Fu1** by the anti-fuel strand **aFu1** releases domain **III** on ring α. The complementarity of domain **II**′ of ring β with **w** and the co-complementarity of the sequences **q** and **p**, associated with ring β, with domain **w** results in the reconfiguration of ring β to domain **w**, to form the energetically stabilized duplex, "state **B**". The transition of ring β to domain **w** unblocks the G-quadruplex sequence, which self-assembles, in the presence of hemin, into the hemin/G-quadruplex DNAzyme structure. The resulting hemin/G-quadruplex DNAzyme catalyzes either the

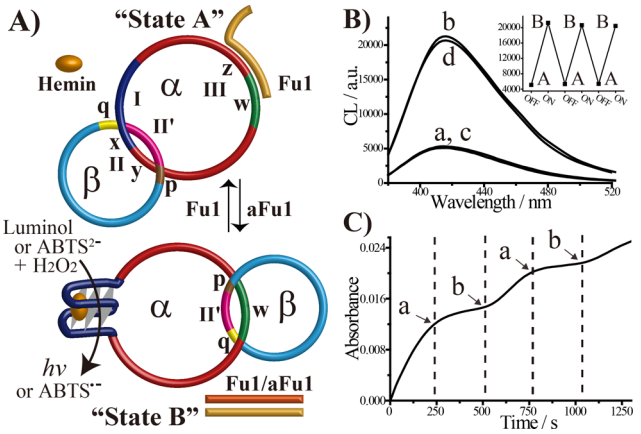

Figure 5. (A) Switchable two-ring interlocked catalytic catenane that implements fuel and anti-fuel strands as triggers. The anti-fuel strand reconfigures the two-ring catenane to yield the hemin/G-quadruplex DNAzyme, switch ON state **B**, while the fuel strand regenerates the catalytic inactive state, switch OFF state **A**. (B) Transduction of the switchable catalytic catenane functions via the hemin/G-quadruplex-catalyzed generation of chemiluminescence (oxidation of luminol by H_2O_2). Curves (a) and (c), the system is in state **A**; curves (b) and (d), the system is in state **B**. Inset: Cyclic chemiluminescence changes upon switching the two-ring catenane across states **A** and **B**. (C) Time-dependent transduction of the switchable catalytic functions of the catenane system through the hemin/G-quadruplex-catalyzed oxidation of $ABTS^{2-}$ by H_2O_2. The system is initiated in state **B**; at times (a) it is transformed to state **A**, and at times (b) it is reconfigured into state **B**. Adapted with permission from ref 32. Copyright 2015 American Chemical Society.

H_2O_2-mediated oxidation of 2,2′-azinobis(3-ethylbenzothiazoline-6-sulfonic acid), $ABTS^{2-}$, to $ABTS^{\bullet-}$ (λ = 415 nm) or the oxidation of luminol by H_2O_2 to generate chemiluminescence (λ = 420 nm). Further displacement of ring β from the domain **w** by the fuel-strand **Fu1** results in the reconfiguration of ring β on the domains **x** and **y** associated with ring α to yield state **A**, where the hemin/G-quadruplex catalytic structure is dissociated into a partially blocked configuration that lacks catalytic activities.

By the sequential treatment of the two-ring catenane structure with the anti-fuel strand, **aFu1**, and fuel strand, **Fu1**, the system is cycled between catalytically active (switch "ON") and inactive (switch "OFF") states, respectively. The catalyzed ON/OFF generation of chemiluminescence, Figure 5B and inset, or the catalyzed ON/OFF oxidation of $ABTS^{2-}$ by H_2O_2 to $ABTS^{\bullet-}$, Figure 5C, provides optical signals for probing the switchable catalytic functions of the catenane.

This concept has been extended to design a two-ring catenane exhibiting dual-switchable catalytic function, a "bis-DNAzyme pendulum",[32] Figure 6A. The two-ring catenane is composed of rings α and β, where ring α includes the domain **I**, composed of sequence **g**, domain **II**, composed of sequence **d**, and domain **III**, comprising sequences **e** and **f**. Domains **I** and **II** associated with ring α correspond to the Mg^{2+}-dependent DNAzyme and the Zn^{2+}-dependent DNAzyme, respectively. The complementarity between domain **III**′ of ring β and the sequences **d** and **e** of ring α results in the formation of state **A**, where, in the presence of ions Mg^{2+} and Zn^{2+}, only the Mg^{2+}-dependent DNAzyme is activated and the Zn^{2+}-dependent DNAzyme is switched OFF due to the partial blocking of the Zn^{2+}-dependent DNAzyme by the ring β. Under these conditions, the Mg^{2+}-dependent DNAzyme cleaved the

DOI: 10.1021/jacs.6b00694
J. Am. Chem. Soc. 2016, 138, 5172–5185

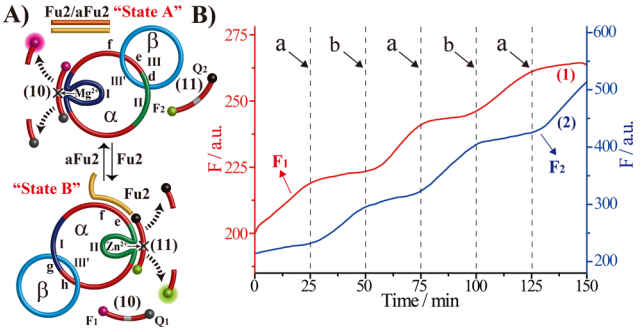

Figure 6. (A) Fuel/anti-fuel-triggered switchable reconfiguration of an interlocked catenane between two catalytic metal-ion-dependent DNAzymes, where in "state **A**" the Mg^{2+}-dependent DNAzyme is switched ON and in "state **B**" the Zn^{2+}-dependent DNAzyme is switched ON. The fluorescence signals of the fluorophore-modified fragmented substrates generated by the different DNAzymes provide the readout for the switchable catalytic functions of the supramolecular device. (B) Time-dependent fluorescence changes of the fluorophore $\mathbf{F_1}$(ROX) and $\mathbf{F_2}$(FAM) upon the switchable reconfiguration of the system between the two states. The process is initiated with the system in state **A**, resulting in the activation of the Mg^{2+}-dependent DNAzyme and the generation of the fluorescence $\mathbf{F_1}$. Subjecting state **A** to the fuel strand **Fu2** reconfigures the system to the Zn^{2+}-dependent catalytic catenane that yields the switched ON fluorescence of $\mathbf{F_2}$, and the switched OFF fluorescence of $\mathbf{F_1}$. Further treatment of the system with the anti-fuel strand **aFu2** regenerates the catalytic state **A**, where $\mathbf{F_1}$ is switched ON and $\mathbf{F_2}$ is switched OFF. Adapted with permission from ref 32. Copyright 2015 American Chemical Society.

fluorophore/quencher $\mathbf{F_1}$(ROX)/$\mathbf{Q_1}$(BHQ-2)-modified substrate **10**, giving rise to the fluorescence of the fragmented $\mathbf{F_1}$–nucleic acid product. Treatment of the two-ring catenane with the fuel-strand **Fu2** displaced ring β from domain **III**, associated with ring α due to the preferential binding of the fuel strand to domains **e** and **f** on ring α. The displaced ring β underwent a transition to the sequences **g** and **h**, associated with ring α (sequence **g** is part of the Mg^{2+}-dependent DNAzyme), resulting in dissociation of the Mg^{2+}-dependent DNAzyme sequence and formation of state **B**. Reconfiguration of state **A** into state **B** released sequence **II** of ring α, resulting in activation of the Zn^{2+}-dependent DNAzyme. Under these conditions, the Zn^{2+}-dependent DNAzyme catalyzed the cleavage of the $\mathbf{F_2}$ (FAM)/$\mathbf{Q_2}$ (IBFQ)-functionalized nucleic acid **11**, while the activity of the Mg^{2+}-dependent DNAzyme was switched OFF. The resulting fluorescence of the $\mathbf{F_2}$-labeled fragmented product provided the readout signal for the activity of the Zn^{2+}-dependent DNAzyme. Subsequent treatment of state **B** with the anti-fuel strand **aFu2** regenerated the energetically stabilized state **A**, where the Mg^{2+}-dependent DNAzyme was switched ON and the Zn^{2+}-dependent DNAzyme was switched OFF. By the sequential treatment of the system with the fuel, **Fu2**, and the anti-fuel, **aFu2**, strands, the cyclic activation of the "bis-DNAzyme pendulum" was demonstrated, Figure 6B. The alternating ON/OFF operation of the two DNAzymes was transduced by the time-dependent fluorescence changes of $\mathbf{F_1}$ and $\mathbf{F_2}$.

3. THREE-, FIVE-, AND SEVEN-RING INTERLOCKED CATENANE NANOSTRUCTURES

Increasing the number of interlocked catenated rings increases the number of structural transitions in the systems. Figure 7A depicts the synthesis of a three-ring catenane, composed of

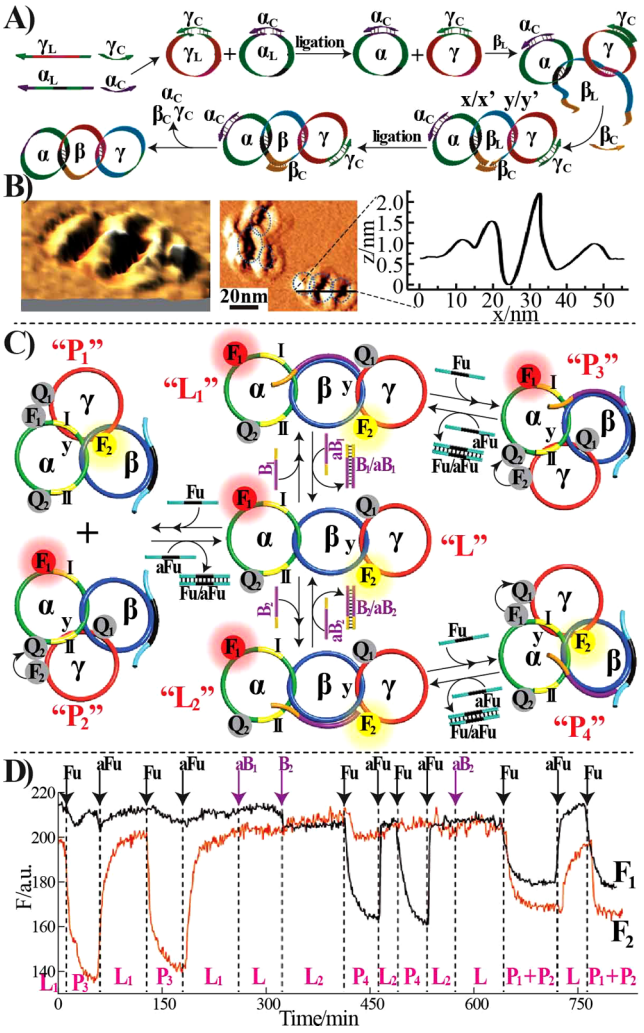

Figure 7. (A) Synthesis of a three-ring interlocked DNA catenane. (B) AFM image and cross-section analysis of the three-ring catenane system. (C) Dictated switchable and reversible reconfiguration of the linear three-ring catenane system **L** into the structures $\mathbf{P_1}$ and $\mathbf{P_2}$ using the fuel/anti-fuel strands, and into the structures $\mathbf{P_3}$ and $\mathbf{P_4}$ using the respective fuel/anti-fuel strands and the blocker/anti-blocker strands as selectors. The topological transitions of the rings are probed by the fluorescence intensities of $\mathbf{F_1}$ and $\mathbf{F_2}$, where ring α is labeled with the fluorophore $\mathbf{F_1}$ and the quencher $\mathbf{Q_2}$, and ring β is labeled with the fluorophore $\mathbf{F_2}$ and the quencher $\mathbf{Q_1}$. (D) Parallel time-dependent fluorescence changes of $\mathbf{F_1}$ and $\mathbf{F_2}$ upon the sequential reconfiguration of the three-ring catenane across the different states. Adapted with permission from ref 23a. Copyright 2012 Wiley-VCH.

rings α, β, and γ.[23a] The synthesis is based on the initial synthesis of the rings α and γ by mixing the linear strands α_L, γ_L with the respective capping strands α_C, γ_C, followed by enzymatic ligation. In the next step, the linear DNA sequence β_L, which forms duplex domains **x**/**x**′ and **y**/**y**′ with rings α and γ respectively, is added to the mixture. Subsequent capping of the inter-threaded strand with β_C, followed by ligation, and denaturing electrophoretic purification, which separates the caps and the non-interlocked rings, yield the linear $\alpha/\beta/\gamma$ three-ring catenane, stabilized by the duplexes **x**/**x**′ and **y**/**y**′. The structure was imaged by AFM, which demonstrated interlocked three-ring structures, Figure 7B, and cross-section analysis of the structures revealed single-strand/double-strand/double-strand/single-strand heights of the interlocked DNA rings.

DOI: 10.1021/jacs.6b00694
J. Am. Chem. Soc. 2016, 138, 5172−5185

The linear three-ring catenane was designed to include in ring α two identical sequences, **I** and **II**, exhibiting complementarity to the domain **y** of ring γ. The enhanced stability of the duplex **y**/**y**′ favors the linear three-ring structure of the system, **L**. Subjecting structure **L** to the fuel-strand, **Fu**, displaces ring γ, and the separated ring γ undergoes dynamic transitions above and beyond the rims of the central ring β to form the structures $\mathbf{P}_1$ and $\mathbf{P}_2$, stabilized by the less favored duplexes, **y**/**I** and **y**/**II**, Figure 7C. The identical composition of sequences **I** and **II** suggests the formation of equimolar concentrations of $\mathbf{P}_1$ and $\mathbf{P}_2$. The dictated transition of ring γ under the lower rim of ring β to form the structure $\mathbf{P}_3$, or the transition of ring γ above the upper rim of ring β to form the structure $\mathbf{P}_4$, was demonstrated by the use of appropriate blocker units. Blocking of the upper rim with the strand $\mathbf{B}_1$ dictates the transition of ring γ across the lower rim of ring β, whereas blocking of the lower rim of ring β with the blocker $\mathbf{B}_2$ stimulated the selective reconfiguration of ring γ along the upper rim of ring β to form the structure $\mathbf{P}_4$. By applying the appropriate anti-blocker and anti-fuel strands, the reconfiguration of structures $\mathbf{P}_3$ and $\mathbf{P}_4$ to the linear three-ring assembly proceeds, and the dynamic inter-conversion across the structures **L**, $\mathbf{P}_1$, $\mathbf{P}_2$, $\mathbf{P}_3$, and $\mathbf{P}_4$ is feasible, Figure 7C. By the labeling of ring α with the fluorophore $\mathbf{F}_1$ and quencher $\mathbf{Q}_2$, and of ring γ with the fluorophore $\mathbf{F}_2$ and quencher $\mathbf{Q}_1$, the dynamic, switchable, and reversible transitions of the system across the configurations **L**, $\mathbf{P}_1$, $\mathbf{P}_2$, $\mathbf{P}_3$, and $\mathbf{P}_4$ were characterized, Figure 7D. For example, while the spatial separation between $\mathbf{F}_1/\mathbf{Q}_2$ and $\mathbf{F}_2/\mathbf{Q}_1$ in structure **L** yields the relatively high fluorescence intensities of the two fluorophores $\mathbf{F}_1$ and $\mathbf{F}_2$, the close proximity between $\mathbf{F}_2/\mathbf{Q}_2$ and spatial separation of $\mathbf{F}_1/\mathbf{Q}_1$ in configuration $\mathbf{P}_3$ yield the relatively high and low fluorescence intensities of $\mathbf{F}_1$ and $\mathbf{F}_2$, respectively. In turn, the blocker/fuel strands-dictated reconfiguration of **L** into structure $\mathbf{P}_4$, resulting in the close proximity between the $\mathbf{F}_1/\mathbf{Q}_1$ pair and the spatial separation between the $\mathbf{F}_2/\mathbf{Q}_2$ pair, which resulted in the low fluorescence intensity of $\mathbf{F}_1$ and relatively high fluorescence intensity of $\mathbf{F}_2$.

Dynamic mechanical transitions of the three-ring catenane machine have been implemented for the programmed organization of gold nanoparticle (Au NP) structures.[33] The three-ring catenane acted as a scaffold for the "mechanical" switchable assembly of the Au NPs, Figure 8A. Toward this end, the linear configuration of the three-ring catenane was functionalized with DNA-conjugated Au NPs. Ring α was modified with 5 nm- and 10 nm-sized Au NPs (functionalized with single nucleic acid strands complementary to the respective sequences on ring α), and ring γ was modified with a 10 nm-sized Au NP. Domains **I** and **II** associated with ring α were complementary to domain **y** of ring γ, and hence, in the presence of the fuel (**Fu**) and respective blocker strands ($\mathbf{B}_1$ or $\mathbf{B}_2$), the dictated programmed reconfiguration of the linear three-Au-NP assembly, $\mathbf{L}_3$, into the NP structures $\mathbf{M}_1$ and $\mathbf{M}_2$ was demonstrated by electron microscopy, Figure 8B. Controlled functionalization of the Au NPs with one or two nucleic acid tethers allowed the stimulated assembly and reconfiguration of three-ring Au NP structures of enhanced complexities, Figure 8C. The rings α of two three-ring catenane systems were cross-linked by bis-nucleic acid-modified 10 nm- and 5 nm-sized Au NPs, and the rings γ of the two catenane scaffolds were modified each with the 10 nm-sized Au NPs to yield the linear structure $\mathbf{L}_4$. The fuel-strand-powered mechanical reconfiguration of $\mathbf{L}_4$, in the presence of the blocker units $\mathbf{B}_1$ or $\mathbf{B}_2$, generated the four-Au-NP isomer

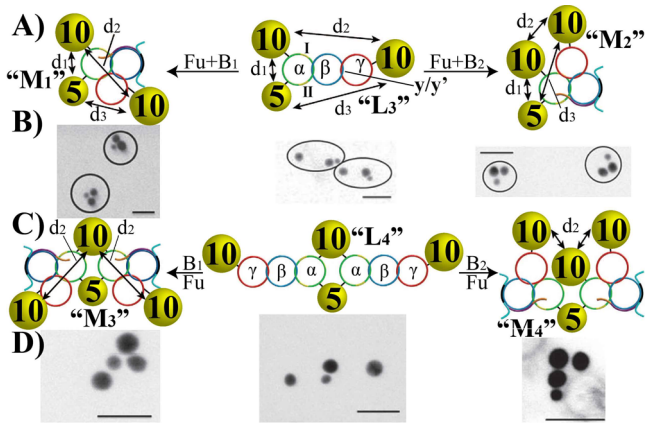

Figure 8. (A) Reconfiguration of three-Au-NP structures using the three-ring catenane as a dynamic scaffold for the organization of the Au NPs, using the respective fuel and blocker strands. The scheme depicts the reconfiguration of the linear structure $\mathbf{L}_3$, consisting of two 10 nm-sized Au NPs and one 5 nm-sized Au NP, into the programmed structures $\mathbf{M}_1$ or $\mathbf{M}_2$, and the calculated interparticle distances are as follow: $\mathbf{L}_3$, $d_1 = 1.5 \pm 0.1$ nm, $d_2 = 14.6 \pm 0.4$ nm, and $d_3 = 10.1 \pm 0.4$ nm; $\mathbf{M}_1$, $d_1 = 1.1 \pm 0.1$ nm, $d_2 = 1.3 \pm 0.1$ nm, and $d_3 = 1.3 \pm 0.1$ nm; $\mathbf{M}_2$, $d_1 = 1.1 \pm 0.1$ nm, $d_2 = 1.3 \pm 0.1$ nm, and $d_3 = 7.2 \pm 0.3$ nm. (B) TEM images corresponding to the Au NP structures $\mathbf{M}_1$, $\mathbf{L}_3$, and $\mathbf{M}_2$ (bars = 25 nm). (C) Reconfiguration of four-Au-NP structures driven by two dynamic scaffolds of the three-ring catenanes cross-linked by a 10 nm- and a 5 nm-sized Au NP. The fuel/blocker-strand-driven dynamic reconfiguration of the linear structure $\mathbf{L}_4$ yields the Au NP structures $\mathbf{M}_3$ or $\mathbf{M}_4$, respectively, exhibiting interparticle distances as follow: $\mathbf{M}_3$, $d_2 = 1.4 \pm 0.6$ nm; $\mathbf{M}_4$, $d_2 = 1.3 \pm 0.1$ nm. (D) TEM images of the structures $\mathbf{M}_3$, $\mathbf{L}_4$, and $\mathbf{M}_4$ (bars = 25 nm). Adapted with permission from ref 33. Copyright 2013 NPG.

structures $\mathbf{M}_3$ and $\mathbf{M}_4$, respectively. TEM images of the resulting Au NPs structures, Figure 8D, demonstrate the formation of dictated nanostructures of Au NPs.

Triggered "mechanical" transitions of the three-ring catenane were also implemented to control the plasmonic interactions between a metal NP and a fluorophore linked to the catenane scaffold,[33] Figure 9A. The linear scaffold $\mathbf{L}_5$ was functionalized on ring α with a fluorophore (Cy3), and ring γ was modified with a 10 nm-sized Au NP. The **Fu**/$\mathbf{B}_1$-stimulated transition of the linear structure under the lower rim of ring β generated the structure $\mathbf{S}_1$, revealing fluorescence quenching of the fluorophore, Figure 9B, curve a. In turn, the **Fu**/$\mathbf{B}_2$-induced transition of the Au NP-modified ring γ across the upper rim of ring β yielded the structure $\mathbf{S}_2$, which revealed fluorescence enhancement of the fluorophore, Figure 9B, curve b. In a control experiment, the linear structure, $\mathbf{L}_5$, was subjected to the **Fu**-strand in the absence of blocker units, and this resulted in negligible fluorescence changes, Figure 9B, curve c, implying that the equimolar concentrations of the resulting structures $\mathbf{S}_1$ and $\mathbf{S}_2$ compensated one another in the fluorescence features of the system. By cyclical treatments of the linear fluorophore/Au NP-modified three-ring catenane $\mathbf{L}_5$ with **Fu**/$\mathbf{B}_1$, **Fu**/$\mathbf{B}_2$, **aFu**/$\mathbf{aB}_1$, and **aFu**/$\mathbf{aB}_2$, the fluorescence features of the system were switched between fluorescence enhancement and fluorescence quenching states, Figure 9C. Figure 9D depicts the theoretically predicted distance-dependent fluorescence properties of Cy3 separated from a 10 nm-sized Au NP. The estimated distances separating the fluorophore from the 10 nm-sized Au NP in structures $\mathbf{S}_1$, $\mathbf{S}_2$, and $\mathbf{L}_5$, and the experimental fluorescence intensities, are consistent with the theoretical predictions.

DOI: 10.1021/jacs.6b00694
J. Am. Chem. Soc. 2016, 138, 5172−5185

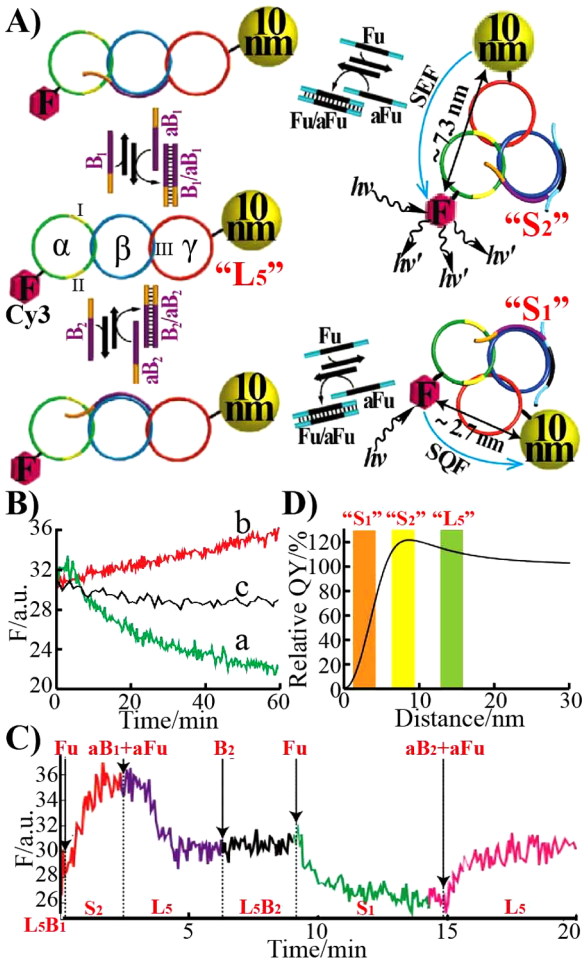

Figure 9. (A) Switchable fluorescence features observed upon the reconfiguration of a three-ring catenane scaffold functionalized with a fluorophore (Cy3) and a 10 nm-sized Au NP. Reversible reconfiguration of the scaffold proceeds across the linear state L_5 and the states S_1 and S_2 using the respective fuel/anti-fuel and blocker/anti-blocker strands. (B) Time-dependent fluorescence changes upon: (a) Reconfiguring the linear L_5 state into the S_1 state, resulting in the quenching of the fluorophore; (b) Reconfiguring the linear L_5 state into the S_2 state, resulting in surface-enhanced fluorescence of the fluorophore; (c) Reconfiguring the linear state L_5, in the absence of blocker strands, into a mixture of S_1 and S_2, resulting in negligible fluorescence changes due to simultaneous quenching and surface-enhanced fluorescence phenomena of the generated structures. (C) Cyclic time-dependent fluorescence changes upon the reconfiguration of the system across the states $L_5 \rightarrow S_2 \rightarrow L_5 \rightarrow S_1 \rightarrow L_5$. (D) Theoretical modeling of the distance-dependent fluorescence properties of the fluorophore Cy3 separated from a 10 nm-sized Au NP. Adapted with permission from ref 33. Copyright 2013 NPG.

These methods for dictating the structures of Au NP aggregates and controlling the fluorescence features of fluorophore/Au NP structures by means of programmed DNA scaffolds were extended to other DNA machines, e.g., tweezers.[34] Stimuli-triggered reconfiguration of a three-ring catenane system was further implemented to design logic gate operations and switchable catalytic systems, Figure 10A.[35] The three-ring linear catenane, $\mathbf{N_1}$, composed of the rings α, β, and γ, was functionalized with the nucleic acids **12**, **13**, **14**, and **15**, modified with the Rhodamine green (RG) fluorophore, $\mathbf{F_1}$ (λ_{em} = 534 nm), and the black-hole quencher, BHQ-1. Ring α was further modified with the duplex nucleic acid **16**/**17**, where nucleic acid **16** is modified with the fluorophore $\mathbf{F_2}$ (Cy3) and the single-strand tether **x** is cytosine-rich, capable of donating an i-motif fragment at acidic pH. Ring γ is modified with the duplex nucleic acid structure **18**/**19**, where **18** is modified with the fluorophore $\mathbf{F_3}$ (Cy5) and includes the cytosine-rich single-stranded tether **y**, capable of donating, at acidic conditions, a subunit for the assembly of an i-motif structure. In the linear structure $\mathbf{N_1}$, the close proximity between $\mathbf{F_1}$ and the quencher BHQ-1 leads to effective quenching of $\mathbf{F_1}$, while the spatial separation between $\mathbf{F_2}$ and $\mathbf{F_3}$ in the structure prohibits any mutual Cy3/Cy5 FRET interactions. Treatment of $\mathbf{N_1}$ with the fuel strands $\mathbf{L_1}$ and $\mathbf{L_2}$ (releasing oligonucleotides (ROs)) results in the strand displacement of rings α and γ from the central ring β, leading to a flexible configuration of the three-ring catenane, $\mathbf{N_2}$, where the fluorophore $\mathbf{F_1}$ units are spatially separated from the BHQ-1 quencher units, whereas the fluorophores $\mathbf{F_2}$ and $\mathbf{F_3}$ are still spatially separated and eliminate mutual FRET interactions. In the catenane configuration $\mathbf{N_2}$, the fluorescence of $\mathbf{F_1}$ is intensified as compared to that in the linear assembly $\mathbf{N_1}$. Subjecting the state $\mathbf{N_2}$ to acidic pH (pH = 5) leads to the rigidification of the catenane into state $\mathbf{N_3}$, where the flexible rings α and γ are interlocked into a rigid configuration by the i-motif bridging structure. In the $\mathbf{N_3}$ state, the $\mathbf{F_1}$/BHQ-1 units are still spatially separated, leading to a relatively high fluorescence of $\mathbf{F_1}$, yet the steric proximity between Cy3 and Cy5 leads to an efficient FRET signal upon excitation of $\mathbf{F_2}$ (Cy3) and the observation of the FRET emission of $\mathbf{F_3}$ (Cy5). The transitions between the states $\mathbf{N_1}$, $\mathbf{N_2}$, and $\mathbf{N_3}$ are reversible, and upon the neutralization of state $\mathbf{N_3}$, the state $\mathbf{N_2}$ is formed. Similarly, treatment of state $\mathbf{N_2}$ with the anti-fuel strands $\mathbf{L_1}'$ and $\mathbf{L_2}'$ displaces the fuel strands $\mathbf{L_1}$ and $\mathbf{L_2}$, leading to the reconfiguration of the linear state $\mathbf{N_1}$. The different states $\mathbf{N_1}$, $\mathbf{N_2}$, and $\mathbf{N_3}$ were impressively imaged by AFM, Figure 10B. The dynamic reconfiguration of the three-ring catenane and the fluorescence features of the different states were translated into logic gate operations. Fuel strands $\mathbf{L_1}$ and $\mathbf{L_2}$ may be considered as a single (united) input, where the acidic pH may act as a second input. The fluorescence properties of $\mathbf{F_1}$, or the FRET signal of $\mathbf{F_3}$, upon the input-triggered reconfiguration of the linear three-ring catenane, $\mathbf{N_1}$, provide the output signals of the respective logic gates. Figure 10C, panel I, depicts the output fluorescence signal of $\mathbf{F_1}$ (λ_{em} = 534 nm) upon subjecting the linear catenane module to the different inputs. The output fluorescence signals are presented as a truth-table, Figure 10C, panel I, inset, that follows the operation of a "YES" logic gate. Similarly, Figure 10C, panel II, shows the fluorescence intensities of the FRET output signal of $\mathbf{F_3}$ (λ_{em} = 663 nm). The resulting fluorescence intensities in the presence of the two inputs are summarized in Figure10C, panel II, inset. These follow an "AND" logic gate operation. By the sequential addition of the ROs, $\mathbf{L_1} + \mathbf{L_2}/\mathbf{L_1}' + \mathbf{L_2}'$, and pH changes, the switchable cyclic reconfiguration of the three-ring catenane across states $\mathbf{N_1}$, $\mathbf{N_2}$, and $\mathbf{N_3}$ was operated, followed by the fluorescence emission of $\mathbf{F_1}$ and $\mathbf{F_3}$, Figure 10D.

The three-ring catenane depicted in Figure 10A was further implemented to develop a switchable catalytic system that follows a SET−RESET logic operation, Figure 11A.[35] Single-stranded nucleic acids **17** and **19**, associated with rings α and γ, respectively, included the G-rich tethers **w** and **z**. Upon the strand displacement of rings α and γ from ring β, in the presence of the fuel strands $\mathbf{L_1}$ and $\mathbf{L_2}$ and under acidic conditions, the linear three-ring catenane $\mathbf{N_4}$ reconfigured into

DOI: 10.1021/jacs.6b00694
J. Am. Chem. Soc. 2016, 138, 5172−5185

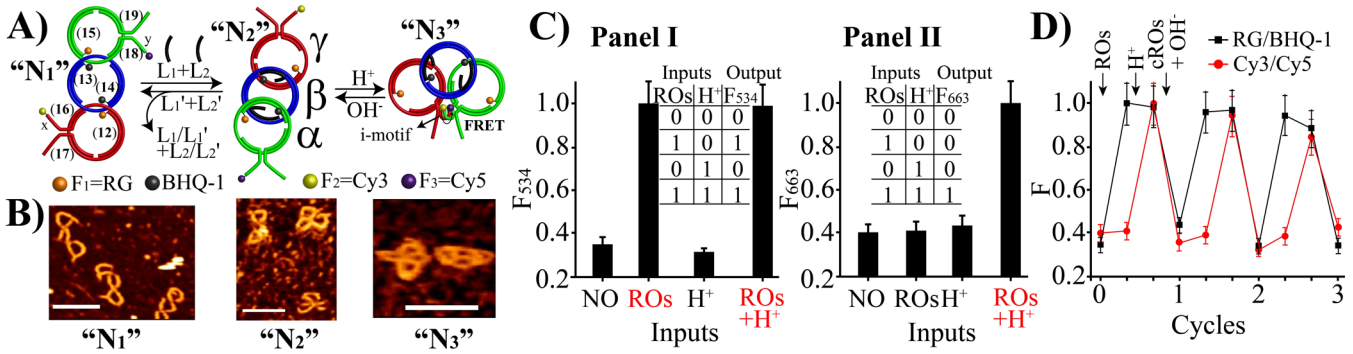

Figure 10. (A) Cascaded switchable reconfiguration of an interlocked three-ring catenane system, $\mathbf{N}_1$, into a flexible three-ring catenane structure, $\mathbf{N}_2$, and back, using two fuel ($\mathbf{L}_1$, $\mathbf{L}_2$) and anti-fuel ($\mathbf{L}_1'$, $\mathbf{L}_2'$) strands, and the subsequent pH-stimulated transition of $\mathbf{N}_2$ into the i-motif-bent configuration $\mathbf{N}_3$ and back. The cyclic switchable transitions of the system were followed by fluorescence spectroscopy via the specific labeling of the catenane with a fluorophore/quencher pair (Rhodamine green (RG)/BHQ-1) and a FRET pair (Cy3/Cy5). (B) AFM images corresponding to the three-ring catenane states $\mathbf{N}_1$, $\mathbf{N}_2$, and $\mathbf{N}_3$ (bar = 50 nm). (C) The cascaded reconfiguration of the three-ring catenane depicted in (A) follows the functions of a logic gate cascade of a "YES" gate (Panel I) and an "AND" gate (Panel II), where the release oligonucleotide strands (ROs) $\mathbf{L}_1$, $\mathbf{L}_2$ act as inputs for the "YES" gate, and the output of the "YES" gate and acidic pH (pH = 5) act as inputs for the "AND" gate. Operation of the "YES" gate in the logic circuit is followed by the fluorescence of RG at 534 nm, and operation of the "AND" gate is probed by the FRET signal at 663 nm. Resetting of the system to state $\mathbf{N}_1$ is accomplished by the implementation of the anti-strands $\mathbf{L}_1'$, $\mathbf{L}_2'$ and/or the anti-strands $\mathbf{L}_1'$, $\mathbf{L}_2'$ and basic pH (pH = 8.0). (D) Cyclic operation of the YES–AND logic circuit probed by the two fluorophores (RG, λ = 534 nm, and Cy5, λ = 633 nm) acting as outputs readout signals. Adapted with permission from ref 35. Copyright 2014 NPG.

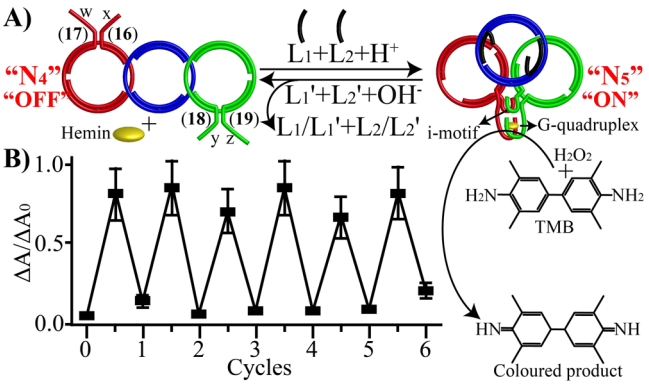

Figure 11. (A) Switchable and reversible reconfiguration of a duplex-functionalized three-ring catenane system using the fuel strands $\mathbf{L}_1$ and $\mathbf{L}_2$ and pH = 5.0 as triggers to transform the linear structure $\mathbf{N}_4$ into the i-motif bent structure $\mathbf{N}_5$, and the reverse process using the anti-fuel strands $\mathbf{L}_1'$ and $\mathbf{L}_2'$ and pH = 8.0 as triggers. The pH-stimulated formation of the i-motif cross-linking units leads to the concomitant assembly of the complement domain, in the presence of K^+ ions, into a G-quadruplex that, in the presence of hemin, yields the hemin/G-quadruplex horseradish peroxidase-mimicking DNAzyme that catalyzed the H_2O_2-mediated oxidation of 3,3′,5,5′-tetramethylbenzidine (TMB) to the colored oxidized product 3,3′,5,5′-tetramethylbenzidine diimine. (B) Absorbance changes resulting upon the cyclic ON and OFF switchable transitions of the catalytic functions of the supramolecular three-ring catenane depicted in (A). Adapted with permission from ref 35. Copyright 2014 NPG.

the bent, i-motif-stabilized structure $\mathbf{N}_5$. The spatial proximity between the tethers **w** and **z** enabled the self-assembly of the G-quadruplex. Binding of hemin to the resulting G-quadruplex resulted in the hemin/G-quadruplex DNAzyme that catalyzed the H_2O_2-mediated oxidation of 3,3′,5,5′-tetramethylbenzidine (TMB) to the colored product 3,3′,5,5′-tetramethylbenzidine diimine. Neutralization of the system in the presence of the anti-fuel strands separated the i-motif bridging units and resulted in the reconfiguration of state $\mathbf{N}_5$ to the linear state structure $\mathbf{N}_4$. This process dissociated the hemin/G-quadruplex structure, leading to a catalytically inactive three-ring catenane configuration. By the cyclic treatment of the system with the fuel strands/H^+ and anti-fuel strands/OH^-, the catalytic functions of the system were switched between the ON and OFF states, respectively, Figure 11B.

Catenanes of enhanced complexities, composed of five interlocked rings[36] and seven interlocked rings,[37] were synthesized. Although the yield of the synthesized interlocked catenanes decreases with increasing number of rings, methods to enhance the final yields of the product were developed. For example, Figure 12A depicts the synthesis of the five-ring catenane. Two two-ring catenanes, $\mathbf{R}_1/\mathbf{R}_2$ and $\mathbf{R}_4/\mathbf{R}_5$, were synthesized and purified. The two catenanes were subjected to the "helper" strand $\mathbf{H}_1$, the strand **x**, and the strand $\mathbf{L}_3$. The "helper" strand $\mathbf{H}_1$ is complementary to domains associated with rings $\mathbf{R}_2$ and $\mathbf{R}_4$, and its hybridization with these two domains brings together $\mathbf{R}_1/\mathbf{R}_2$ and $\mathbf{R}_4/\mathbf{R}_5$ into a supramolecular template for the synthesis of the five-ring catenane. The sequence $\mathbf{L}_3$ hybridizes with complementary domains of rings $\mathbf{R}_2$ and $\mathbf{R}_4$, and the hybridization of the strand **x** with a domain associated with $\mathbf{L}_3$ rigidifies $\mathbf{L}_3$, thus favoring the intermolecular threading of $\mathbf{L}_3$ into a quasi-circular supramolecular assembly consisting of the "helper"-bridged $\mathbf{R}_1/\mathbf{R}_2$ and $\mathbf{R}_4/\mathbf{R}_5$ structures. Subsequent capping of the quasi-circular unit with the capping strand $\mathbf{C}_3$, followed by ligation of the ends of $\mathbf{L}_3$, yielded, after removal of the units $\mathbf{H}_1$, $\mathbf{C}_3$, and **x** and final purification, the five-ring interlocked catenane $\mathbf{R}_1/\mathbf{R}_2/\mathbf{R}_3/\mathbf{R}_4/\mathbf{R}_5$. The resulting catenane was hybridized with fluorophore and quencher units, where the rings $\mathbf{R}_1$ and $\mathbf{R}_5$ were functionalized through hybridization with a Cy3-modified nucleic acid and a Cy5.5-modified nucleic acid, respectively. Ring $\mathbf{R}_3$ was modified, through hybridization, with two quencher-functionalized nucleic acids, the BHQ-2 and IAbRQ quencher units, respectively. The five-ring interlocked catenane underwent cyclic dynamic reconfigurations across four states, **I**, **II**, **III**, and **IV**, upon subjecting the five-ring catenane to strand displacement processes using the four fuel strands $\mathbf{F}_1$, $\mathbf{F}_2$, $\mathbf{F}_3$, and $\mathbf{F}_4$ and the respective anti-fuel strands $\mathbf{aF}_1$, $\mathbf{aF}_2$, $\mathbf{aF}_3$, and $\mathbf{aF}_4$, Figure 12B. The fluorescence intensities of the two fluorophores Cy3 and Cy5.5 provided, then, optical readouts

DOI: 10.1021/jacs.6b00694
J. Am. Chem. Soc. 2016, 138, 5172–5185

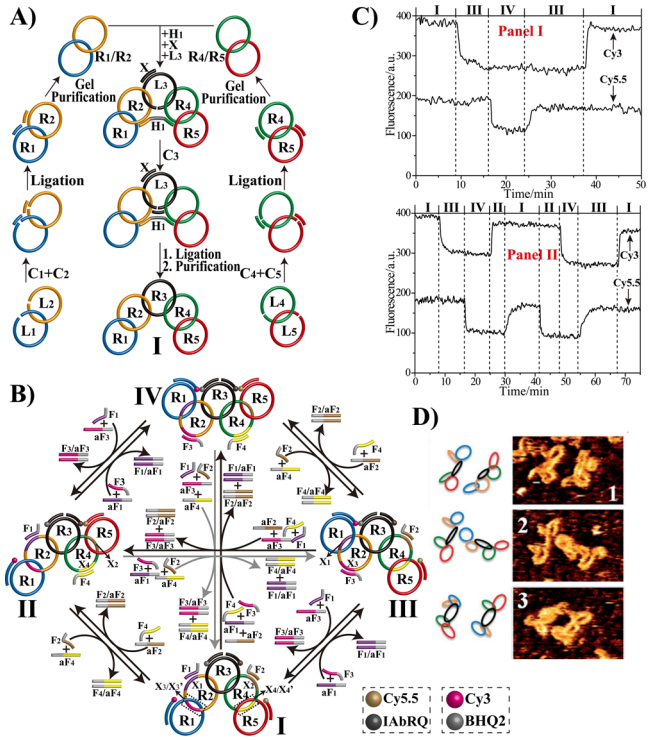

Figure 12. (A) Synthesis of a five-ring interlocked DNA catenane. (B) Reversible reconfiguration of the five-ring interlocked DNA catenane across the states I, II, III and IV using appropriate fuel/anti-fuel strands. The different states are followed by probing the fluorescence features of the two fluorophores Cy3 and Cy5.5 and the quenchers IAbRQ and BHQ-2 as labels. (C) Time-dependent fluorescence changes of the two fluorophores upon the fuel/anti-fuel triggered transitions across states. Panel I: I→III→IV→III→I; Panel II: I→III→IV→II→I→II→IV→III→I. (D) AFM images of the five-ring interlocked catenane structure presenting the "olympiadane" – state IV configuration. Adapted with permission from ref 36. Copyright 2014 Wiley-VCH.

for the reconfiguration of the system across the different states. For example, Figure 12C, panel I, depicts the fluorescence intensities of the two fluorophore labels upon the cyclic transitions of the system across the states **I→III→IV→III→I**, whereas panel II presents the time-dependent fluorescence changes of the fluorophore labels upon the cyclic transitions of the system across the states **I→III→IV→II→I→II→IV→III→I**. The five-ring interlocked DNA catenane in configuration **IV** presents the DNA Olympiadane nanostructure. Besides the dynamic reconfiguration of this nanostructure in the presence of external fuel/anti-fuel strands, the successful imaging of the smallest Olympiadane structure at the single-molecule level was demonstrated, Figure 12D.

The five-ring catenane system was, similarly, used as a scaffold for the cyclic reconfiguration of different sized Au NPs, Figure 13A. The "decoration" of the five-ring catenane in configuration **I**, with a 15 nm-sized Au NP-functionalized oligonucleotide on ring $\mathbf{R_3}$ and two 5 nm-sized Au NP-modified oligonucleotides on rings $\mathbf{R_1}$ and $\mathbf{R_5}$ yielded a Au NP structure exhibiting interparticle distances corresponding to $d_1 \approx 14.5$ nm, $d_2 \approx 25$ nm, and $d_3 \approx 32$ nm, Figure 13B. Transition of the DNA scaffold from state **I** to state **IV**, in the presence of the fuel strands $\mathbf{F_3}$ and $\mathbf{F_4}$ and the anti-fuel strands $\mathbf{aF_1}$ and $\mathbf{aF_2}$, reconfigured the three NPs into a compact structure where the

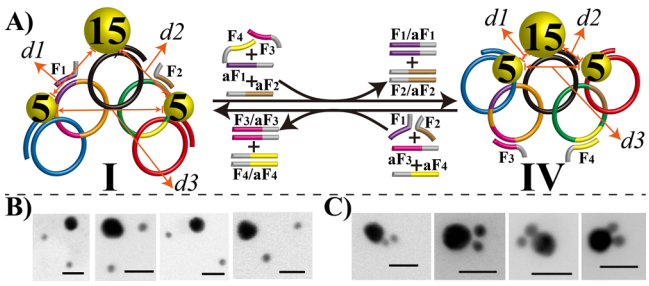

Figure 13. (A) Switchable reconfiguration of three Au NPs (2 × 5 nm, 1 × 15 nm) using the five-ring catenane as dynamic scaffold for the organization of the Au NPs. (B) TEM images of the Au NPs in state **I**. (C) TEM images of the Au NPs in state **IV**. Bar = 20 nm. Adapted with permission from ref 36. Copyright 2014 Wiley-VCH.

interparticle distances corresponded to $d_1 \approx 0.8$ nm, $d_2 \approx 1.5$ nm, and $d_3 \approx 2.0$ nm, Figure 13C.

The synthesis of the seven-ring catenane is displayed in Figure 14A. It involves the primary synthesis of a three-ring catenane, $\mathbf{R_1/R_2/R_3}$, and a single DNA circle, $\mathbf{R_4}$. In the presence of three "helper" strands, $\mathbf{H_{4,5,7}}$, $\mathbf{H_{5,6}}$, and $\mathbf{H_{2,5}}$, and the single strands $\mathbf{L_5}$, $\mathbf{L_6}$, and $\mathbf{L_7}$, the supramolecular structure $\mathbf{T_1}$ is formed, where the strands $\mathbf{L_5}$, $\mathbf{L_6}$, and $\mathbf{L_7}$ are forced into quasi-circle configurations by means of the "helper" units (and the circular $\mathbf{R_1/R_2/R_3}$ and $\mathbf{R_4}$ templates). Capping of the quasi-circle strands with strands $\mathbf{C_5}$, $\mathbf{C_6}$, and $\mathbf{C_7}$, followed by ligation of the strands, led, after purification, to the seven-ring interlocked catenane, structure $\mathbf{T_2}$.

The resulting structure was imaged at the single-molecule level, Figure 14B. The seven-ring interlocked catenane, i.e., the "molecular robot", was designed to include in its structure three fixed rings, $\mathbf{R_2}$, $\mathbf{R_5}$ ("body units"), and $\mathbf{R_7}$ ("head"). Rings $\mathbf{R_1}$, $\mathbf{R_3}$, $\mathbf{R_4}$, and $\mathbf{R_6}$ represent pairs of moveable elements ("legs" and "arms", respectively), Figure 14C. The "arms" and "legs" could be reconfigured separately or cooperatively, using respective fuel and anti-fuel strands. $\mathbf{R_1}$, $\mathbf{R_3}$, $\mathbf{R_4}$, and $\mathbf{R_6}$ were labeled with the fluorophores Cy3, TEX615, Cy5, and Cy5.5, respectively. $\mathbf{R_2}$ and $\mathbf{R_5}$ were each labeled with two identical quencher units, IAbRQ. Reconfigurations of the moving rings $\mathbf{R_1}$, $\mathbf{R_3}$, $\mathbf{R_4}$, and $\mathbf{R_6}$, in the presence of fuel and anti-fuel strands, control the distances separating the different fluorescent labels with respect to the quencher units; thus, the fluorescence intensities of the different fluorophores provide a "fingerprint" for the configuration of the different states. For example, Figure 14D shows the reversible fuel/anti-fuel transitions of state $\mathbf{S_1}$ to states $\mathbf{S_6}$, $\mathbf{S_7}$, $\mathbf{S_8}$, $\mathbf{S_9}$, $\mathbf{S_{10}}$, and $\mathbf{S_{11}}$, upon the concomitant transitions of rings $\mathbf{R_4/R_6}$, $\mathbf{R_3/R_4}$, $\mathbf{R_1/R_6}$, $\mathbf{R_1/R_3}$, $\mathbf{R_1/R_4}$, and $\mathbf{R_3/R_6}$, respectively. Figure 14E presents the time-dependent fluorescence changes upon stimulating this set of transitions. Similarly, Figure 14F shows the reversible switching of $\mathbf{S_1}$ to states $\mathbf{S_{12}}$, $\mathbf{S_{13}}$, $\mathbf{S_{14}}$, and $\mathbf{S_{15}}$ upon the cyclic concomitant transitions of three rings, $\mathbf{R_1/R_4/R_6}$, $\mathbf{R_3/R_4/R_6}$, $\mathbf{R_1/R_3/R_6}$, and $\mathbf{R_1/R_3/R_4}$, respectively. The time-dependent fluorescence changes that occur upon subjecting the system to the appropriate fuel/anti-fuel strands for these transitions are depicted in Figure 14G.

4. INTERLOCKED DNA ROTAXANES

Rotaxanes are supramolecular assemblies consisting of an axle on which a ring–guest molecule is threaded. Different host–guest interactions, such as donor–acceptor,[38] metal ion–ligand,[39] and electrostatic interactions,[40] were applied to

DOI: 10.1021/jacs.6b00694
J. Am. Chem. Soc. 2016, 138, 5172–5185

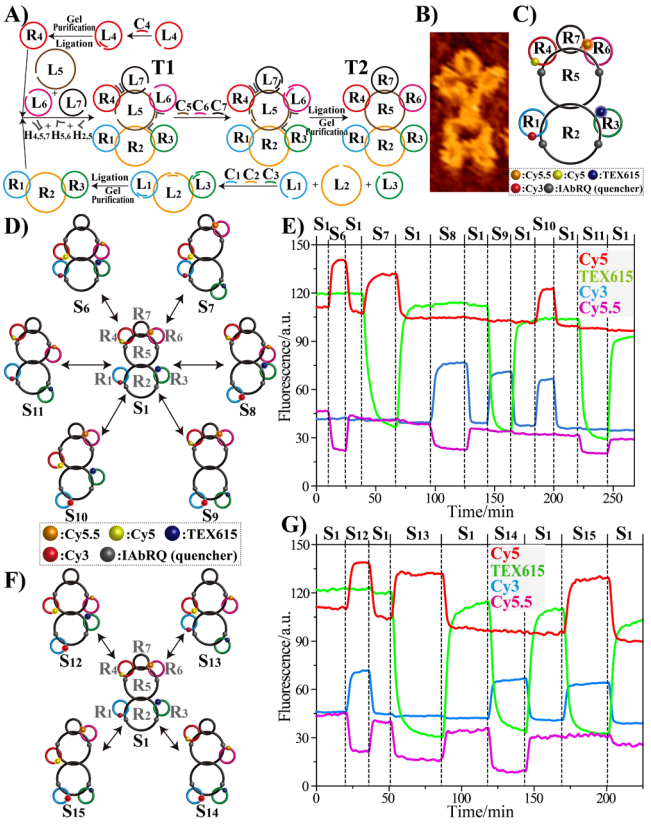

Figure 14. (A) Synthesis of a seven-ring interlocked DNA catenane. (B) AFM image of the seven-ring interlocked catenane. (C) Schematic structure of the seven-ring catenane labeled with four different fluorophores, Cy3, Cy5, Cy5.5, and TEX 615, and the quencher IAbRQ, which allow fluorescence probing of the dynamic reconfigurations of the system. (D) Dynamic reversible reconfiguration of state $\mathbf{S_1}$ to states $\mathbf{S_6}$, $\mathbf{S_7}$, $\mathbf{S_8}$, $\mathbf{S_9}$, $\mathbf{S_{10}}$, and $\mathbf{S_{11}}$ that present examples where two different rings associated with the $\mathbf{S_1}$ state are transformed into new configurations on the catenane scaffold. The transitions are stimulated by appropriate fuel/anti-fuel strands. (E) Time-dependent fluorescence changes of the four fluorophore labels upon the cyclic and reversible reconfiguration of the system across states $\mathbf{S_1} \rightarrow \mathbf{S_6} \rightarrow \mathbf{S_1} \rightarrow \mathbf{S_7} \rightarrow \mathbf{S_1} \rightarrow \mathbf{S_8} \rightarrow \mathbf{S_1} \rightarrow \mathbf{S_9} \rightarrow \mathbf{S_1} \rightarrow \mathbf{S_{10}} \rightarrow \mathbf{S_1} \rightarrow \mathbf{S_{11}} \rightarrow \mathbf{S_1}$. (F) Examples for the reversible reconfiguration of three different rings, associated with state $\mathbf{S_1}$, to yield in the presence of appropriate fuel/anti-fuel strands the states $\mathbf{S_{12}}$, $\mathbf{S_{13}}$, $\mathbf{S_{14}}$, and $\mathbf{S_{15}}$. (G) Time-dependent fluorescence changes corresponding to the four fluorophore labels, associated with the seven-ring catenane, upon the cyclic and reversible reconfiguration of the seven-ring catenane system across the states $\mathbf{S_1} \rightarrow \mathbf{S_{12}} \rightarrow \mathbf{S_1} \rightarrow \mathbf{S_{13}} \rightarrow \mathbf{S_1} \rightarrow \mathbf{S_{14}} \rightarrow \mathbf{S_1} \rightarrow \mathbf{S_{15}} \rightarrow \mathbf{S_1}$. Adapted with permission from ref 37. Copyright 2015 American Chemical Society.

stabilize the threaded configuration of the guest molecule on the axle. Stoppering of the axle ends with bulky molecular or macromolecular components leads, then, to a non-separable supramolecular structure termed rotaxane. By pre-designing stimuli-responsive binding sites for the ring component on the axle, the triggered cyclic and switchable programmed transitions of the ring across distinct sites were demonstrated.[41] Different external triggers, such as pH, light, or electrical stimuli, were reported to shuttle the rotaxane ring on the axle in solution or on surfaces.[42] Several excellent review articles have addressed the developments in supramolecular rotaxane chemistry.[43] Advances in the synthesis of interlocked DNA rings were accompanied by the development of methods to assemble supramolecular DNA rotaxane structures. By one method,[44]

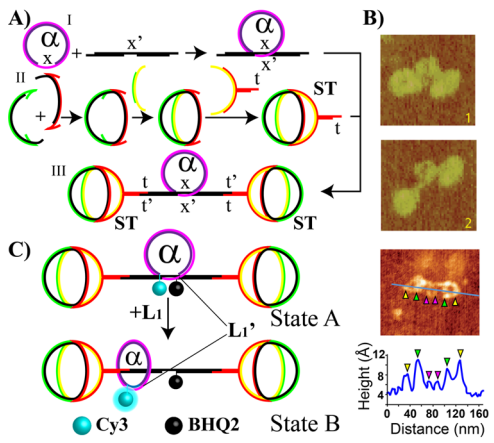

Figure 15. (A) Stepwise assembly of a double-stranded rotaxane system. (B) AFM image and cross-section analysis of the resulting rotaxane. (C) Reconfiguration of ring α on the axle of the rotaxane structure, using the fuel strand $\mathbf{L_1}$. The reconfiguration process is followed by fluorescence spectroscopy via labeling the ring α with the fluorophore Cy3 and the axle with the quencher BHQ-2. Adapted with permission from ref 44. Copyright 2010 NPG.

Figure 15A panel I, the circular DNA ring α was inter-threaded on a DNA axle using base-pair complementarity between domains **x** and **x′** associated with the ring and the axle, respectively. Spherical DNA stopper units **ST** were prepared by the stepwise assembly of quarter-sphere, hemisphere, and spherical stoppers consisting of 15 individual strands exhibiting programmed complementarity, Figure 15A, panel II. A single-strand tether **t** linked to the stopper units, and its hybridization to the domain **t′**, provides a means to assemble the stoppered rotaxane structure, Figure 15A, panel III. Figure 15B depicts representative AFM images of the rotaxane structures. Cross-section analysis reveals the approximate length of the rotaxane structure to be 70 nm and the height of the stopper units to be substantially larger than the threaded ring unit, as expected from the geometry of the DNA duplex and the specific sequence design. Treatment of the rotaxane assembly with a fuel strand, $\mathbf{L_1}$, resulted in the displacement of ring α through the stabilization of the duplex between $\mathbf{L_1}$ and the domain $\mathbf{L_1'}$ associated with the ring. This resulted in the shuttling of the ring on the axle, Figure 15C. Reconfiguration of ring α on the rotaxane axle was probed by following the fluorescence changes of a fluorophore/quencher pair acting as labels on the ring and axle, respectively.

A further DNA rotaxane system that revealed enhanced rigidity was assembled by reinforcing the axle unit using a PX100 crossover structure, Figure 16A.[45] The rigidified axle was threaded into the ring **R** through the hybridization of the ring to the axle. The resulting supramolecular structure was then stoppered by bulky spherical DNA units to yield the rotaxane. Figure 16B depicts the AFM images of the rotaxane system. The length of the imaged rotaxane structure fits well the estimated calculated value of ca. 93 nm.

In a similar system, the reversible shuttling of the rotaxane ring on the axle unit was demonstrated in the presence of fuel/anti-fuel strands or by the reversible photoisomerization of azobenzene units that controlled the binding features of the rotaxane ring to the axle, Figure 17A,B.[46] Rotaxane ring **R** was hybridized with a single-strand domain of the axle, and the structure was stoppered by two bulky spherical blocker units, to yield the "firm" rotaxane structure, state **A**. In the presence of

DOI: 10.1021/jacs.6b00694
J. Am. Chem. Soc. 2016, 138, 5172−5185

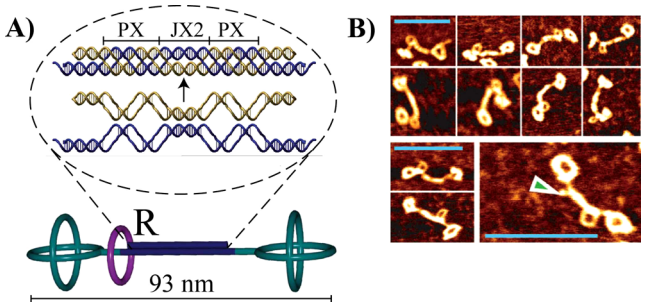

Figure 16. (A) Schematic structure of a DNA rotaxane, analogous to the rotaxane in Figure 15, where the axle unit is rigidified by a PX100 crossover motif. (B) AFM image of the resulting rotaxane structure, bar = 100 nm. Adapted with permission from ref 45. Copyright 2012 Wiley-VCH.

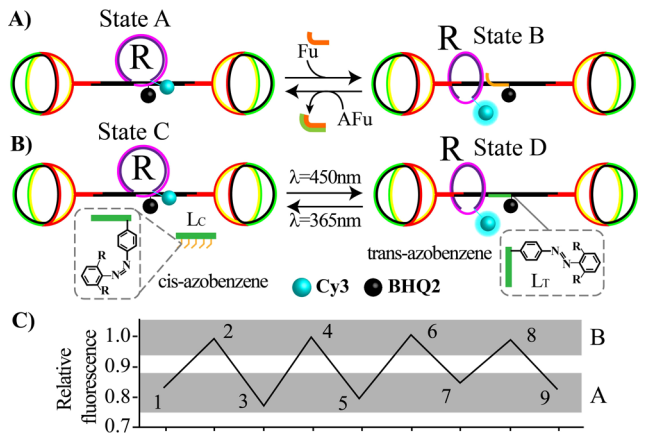

Figure 17. (A) Fuel (Fu)/anti-fuel (AFu)-driven switchable reconfiguration of a circular DNA (**R**) on a rotaxane axle between states **A** and **B**. The switching processes are followed by a fluorophore/quencher pair modifying the nanostructure. (B) Light-induced switchable reconfiguration of a circular DNA (**R**) between states **C** and **D**, using a photoisomerizable azobenzene-modified strand as switching promoter. In the presence of the *trans*-azobenzene strand $\mathbf{L_T}$, the ring is displaced to state **D**, while photoisomerization to the *cis*-azobenzene strand $\mathbf{L_C}$ regenerated the energetically stabilized state **C**. The switching process is followed using a fluorophore/quencher pair that modifies the nanostructure. (C) Switchable fluorescence changes upon the reconfiguration of the rotaxane structure between states **A** and **B**, respectively. Adapted with permission from ref 46. Copyright 2012 American Chemical Society.

the appropriate trigger, ring **R** is displaced to yield a "mobile" configuration of the ring on the axle, state **B**. By labeling the ring with a fluorophore (Cy3) and the axle with a quencher unit (BHQ-2), the reconfiguration of the rotaxane could be followed. In the firm configuration, state **A**, the close proximity between the fluorophore and quencher unit led to the effective fluorescence quenching of Cy3, whereas the spatial separation between the fluorophore and quencher units in the "mobile" rotaxane configuration, state **B**, led to the intensified fluorescence of Cy3. Figure 17A depicts the schematic strand displacement of the ring from state **A**, using the fuel strand, and the recovery of the non-mobile configuration, state **B** to state **A**, upon the displacement of the fuel strand with the respective anti-fuel strand.

Figure 17B presents the light-induced shuttling of the rotaxane ring **R** within the supramolecular structure. The synergistic effect of the *trans*-azobenzene intercalators on the stability of duplex nucleic acids was used as the driving force to shuttle the rotaxane system. The system consisted of the firm rotaxane structure and the *cis*-azobenzene-modified strand $\mathbf{L_C}$. Under these conditions, the strand displacement of the ring is prohibited due to insufficient stabilization of the duplex $\mathbf{L_C}$-axle, state **C**. Photoisomerization of the *cis*-azobenzene-modified strand (λ = 450 nm) $\mathbf{L_C}$ to the *trans*-azobenzene fuel-strand $\mathbf{L_T}$, leads to the displacement of the ring due to the cooperative stabilization of the duplex between $\mathbf{L_T}$ and the axle by the *trans*-azobenzene intercalator units, leading to the mobile configuration, state **D**. By the reverse photoisomerization of $\mathbf{L_T}$ to $\mathbf{L_C}$ (λ = 365 nm), the duplex between $\mathbf{L_C}$ and the axle is separated, leading to the re-formation of state **C**. By the cyclic photoisomerization of the fuel-strand between the $\mathbf{L_C}$ and $\mathbf{L_T}$ photoisomers, the rotaxane system was reversibly switched between the firm (state **C**) and the mobile (state **D**) configurations, respectively. Figure 17C shows the cyclic fluorescence changes of the system upon its treatment with the fuel/anti-fuel strands. DNA rotaxane nanostructures exhibiting enhanced complexity, e.g., threading of two rings[47] on the rotaxane axle, were reported. Separation of the rotaxane ring by different input triggers, such as strand displacement or light, was implemented to operate logic gates by these systems.[47]

A different method to prepare reconfigurable DNA rotaxanes has implemented Au NPs as stoppers, Figure 18, Panel I, (A).[48] Axle **20** was modified at its 3′ and 5′ ends with thiol functionalities, and it included three domains, **I**, **II**, and **III**. Strand **20** was interacted with the circular DNA **21** that includes an encoded sequence complementary to domains **I** and **II** of the axle, and domain **II** on the axle was blocked with the nucleic acid strand **22**. Since domain **II** was blocked by **22**, the axle can inter-thread into the ring to form an interlocked pseudo-rotaxane structure with ring **20** (or alternatively form a kissing duplex between the axle and ring). Subsequently, the pseudo-rotaxane system was interacted with the strand **23** that is complementary to domain **III** of the axle, to yield a rigidified pseudo-rotaxane structure. The bis-thiolated pseudo-rotaxane structure was then interacted with 10 nm-sized Au NPs to yield the Au NP-stoppered rotaxane between ring **21** and the rigidified axle. After gel electrophoretic removal of the ring unit in kissing interaction, and upon addition of anti-blocker strands **22*** and **23*** that remove the blocker units, the rotaxane structure that includes free domains **II** and **III** was formed. Formation of the interlocked hybrid rotaxane between ring **21** and the axle was confirmed by the selective attachment of 15 nm- or 5 nm-sized Au NPs, functionalized with the nucleic acid **24**, complementary to a single-stranded domain of ring **21**, and imaging the three NP aggregates by transmission electron microscopy (TEM), Figure 18, Panel I, (B) and (C).

The Au NP-stoppered DNA rotaxane was applied as a scaffold for the reversible reconfiguration of the DNA ring on the rotaxane axle, Figure 18, Panel II. Reconfiguration of the ring was followed by the labeling of the reconfigured ring with auxiliary fluorophore-functionalized strands **25** or **26** that probe the dynamic shuttling of the ring on the axle via the interactions between the fluorophore and the Au NP-stopper units. Using the appropriate fuel and anti-fuel strands, the DNA rotaxane ring could be shuttled from domain **I** to domain **II** (states **A** and **B**, respectively) associated with the axle, and back, using the strand displacement mechanism. Using the 3′-Cy3-modified strand **25** as label, shuttling of the rotaxane from domain **I** to **II** resulted in the fluorophore quenching, and by the reversible

DOI: 10.1021/jacs.6b00694
J. Am. Chem. Soc. 2016, 138, 5172−5185

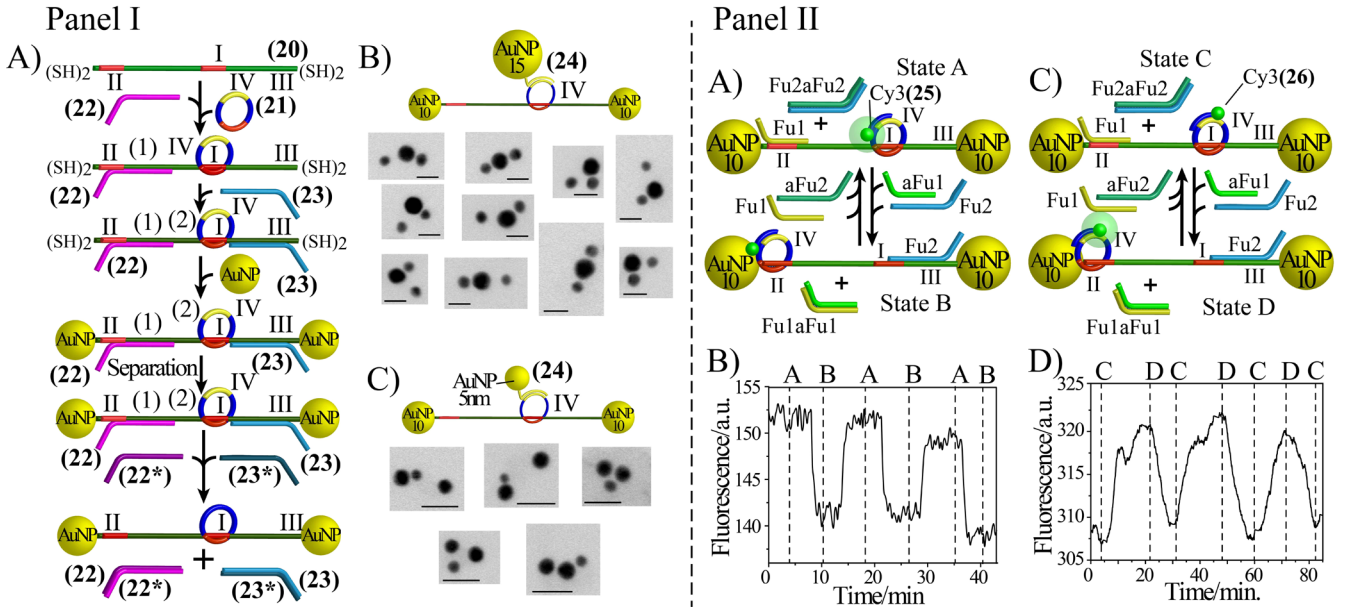

Figure 18. Panel I: (A) Synthesis of a DNA rotaxane stoppered by two 10 nm-sized Au NPs. (B) TEM images corresponding to the organization of three Au NPs on the rotaxane scaffold via the hybridization of a 15 nm-sized Au NP-functionalized strand with the ring of the rotaxane structure stoppered by two 10 nm-sized NPs (bar = 20 nm). (C) TEM images corresponding to the organization of three Au NPs on the rotaxane scaffold via the hybridization of a 5 nm-sized Au NP-functionalized strand with the ring of the rotaxane structure, stoppered by two 10 nm-sized NPs (bar = 20 nm). Panel II: (A) Functionalization of the ring associated with the rotaxane scaffold with a 3′-fluorophore-functionalized strand **25** (fluorophore = Cy3), and the cyclic reconfiguration of the ring between states **A** and **B** using fuel and anti-fuel strands. The switchable reconfiguration of the rotaxane structures is followed by the fluorescence quenching of the fluorophore by the Au NP stopper. (B) Time-dependent fluorescence changes upon the cyclic fuel/anti-fuel triggered transition between states **A** and **B**. (C) Functionalization of the ring associated with the rotaxane scaffold with a 5′-fluorophore-functionalized strand, **26** (fluorophore = Cy3), and the cyclic reconfiguration of the ring between states **C** and **D** using fuel and anti-fuel strands—the switchable reconfiguration of the rotaxane structures is followed by the surface-enhanced fluorescence of the fluorophore by the Au NP stopper. (D) Time-dependent fluorescence changes upon the cyclic fuel/anti-fuel triggered transitions between states **C** and **D**. Adapted with permission from ref 48. Copyright 2013 American Chemical Society.

reconfiguration of the ring between domains **I** and **II**, cyclic fluorescence quenching and restoration of the original fluorescence were observed, Figure 18, Panel II, (A) and (B). In turn, the implementation of the 5′-Cy3-modified strand **26** as auxiliary label revealed that the transition of the ring from domain **I** to domain **II** (states **C** and **D**, respectively), associated with the axle, resulted in the surface-enhanced fluorescence of the fluorophore emission, Figure 18, Panel II, (C) and (D). Theoretical calculations indicated that the spatial separation between the Cy3 fluorophore in strand **26**, from the plasmonic Au NP stopper surface, is at the appropriate distance to yield the plasmonic induced surface enhanced fluorescence.

5. CONCLUSIONS AND PROSPECTIVES

This Perspective has demonstrated the advances in synthesizing stimuli-responsive, reconfigurable, interlocked catenane and rotaxane systems. The successful synthesis of three-, five-, and seven-ring catenanes was discussed, and approaches to synthesize DNA rotaxanes stoppered by bulk oligonucleotide stoppers or metal nanoparticle stoppers were addressed. Different triggers to reversibly reconfigure catenane or rotaxane systems were introduced, such as fuel/anti-fuel strands, metal ion/ligands, variable pH stimuli, and light signals. Reconfiguration of the interlocked structures allowed the operation of DNA devices such as rotors, a pendulum, and shuttles. Also, the dynamic reconfiguration of interlocked DNA scaffolds enabled the switchable reconfiguration of metallic nanoparticle structures and the control of plasmonic effects, e.g. surface-enhanced fluorescence, dictated by the catenane/rotaxane scaffolds. Furthermore, the switching of catalytic reactions between ON and OFF states by means of reconfigurable catenanes was demonstrated. At present, the synthesis of interlocked DNA structures is limited by the low yields of the products. Improvement of the synthetic route to prepare these compounds, and eventually the engineering of organisms that manufacture the catenane/rotaxane structures as genomic materials, are challenges for the future.

Besides fundamental basic studies related to interlocked catenane/rotaxane structures, such as probing the forces stabilizing the interlocked structures by AFM,[49] or imaging the transport properties of interlocked structures through nanopores,[50] the application of these structures is a future challenge. While the reconfiguration of DNA catenanes/rotaxanes by analyte genes or aptamer−ligand complexes, and the optical (fluorescence) transduction of the reconfiguration processes, seem to be natural possibilities to develop different sensor devices, more complex applications can be envisaged. For example, strand-dictated reconfigurable multi-ring catenanes provide a rich arena of different states that could act as functional elements for computing automata[51] or as a scaffold for multi-valued logics.[52] Furthermore, the fact that circular DNAs lack 3′ and 5′ termini suggests that such structures, and particularly catenanes that include non-natural nucleotide bases, should reveal enhanced stabilities toward enzymatic degradation, as compared to linear analogues. Thus, such interlocked structures could function as useful intracellular imaging agents and eventually sense-and-treat intracellular machines. For example, the intracellular biomarker-induced activation of

DOI: 10.1021/jacs.6b00694
J. Am. Chem. Soc. 2016, 138, 5172−5185

DNAzyme-functionalized catenanes, e.g., by aptamer–ligand interactions, could lead to specific RNA cleavage and control of cell proliferation. Furthermore, the catenane and rotaxane structures operate at present as diffusional switchable devices. Immobilization of the supramolecular DNA devices on surfaces could be an interesting path to follow. Specifically, the modification of surfaces with a single-stoppered DNA quasi-rotaxane could yield a functional scaffold for the switchable electrical wiring of redox proteins,[53] native photosystems,[54] or semiconductor quantum dots,[55] leading to new bioelectronic or photoelectrochemical DNA-based devices.

AUTHOR INFORMATION

Corresponding Author

*willnea@vms.huji.ac.il

Notes

The authors declare no competing financial interest.

ACKNOWLEDGMENTS

Our research on interlocked DNA devices was supported by the Israel Science Foundation, the Volkswagen Foundation, Germany, and by the Minerva Center of Biohybrid Complex Systems.

REFERENCES

(1) Wang, F.; Lu, C.-H.; Willner, I. *Chem. Rev.* **2014**, *114*, 2881.

(2) (a) SantaLucia, J.; Hicks, D. *Annu. Rev. Biophys. Biomol. Struct.* **2004**, *33*, 415. (b) Zhang, D. Y.; Turberfield, A. J.; Yurke, B.; Winfree, E. *Science* **2007**, *318*, 1121. (c) Soloveichik, D.; Seelig, G.; Winfree, E. *Proc. Natl. Acad. Sci. U. S. A.* **2010**, *107*, 5393.

(3) (a) Yurke, B.; Mills, A. P. *Genet. Program. Evolvable Machines* **2003**, *4*, 111. (b) Li, Q.; Luan, G.; Guo, Q.; Liang, J. *Nucleic Acids Res.* **2002**, *30*, e5. (c) Zhang, D. Y.; Seelig, G. *Nat. Chem.* **2011**, *3*, 103.

(4) (a) Gehring, K.; Leroy, J. L.; Gueron, M. *Nature* **1993**, *363*, 561. (b) Collin, D.; Gehring, K. *J. Am. Chem. Soc.* **1998**, *120*, 4069. (c) Leroy, J. L.; Gueron, M.; Mergny, J. L.; Helene, C. *Nucleic Acids Res.* **1994**, *22*, 1600. (d) Nonin, S.; Leroy, J. L. *J. Mol. Biol.* **1996**, *261*, 399.

(5) (a) Leitner, D.; Schroder, W.; Weisz, K. *Biochemistry* **2000**, *39*, 5886. (b) Asensio, J. L.; Lane, A. N.; Dhesi, J.; Bergqvist, S.; Brown, T. J. *J. Mol. Biol.* **1998**, *275*, 811. (c) Soto, A. M.; Loo, J.; Marky, L. A. *J. Am. Chem. Soc.* **2002**, *124*, 14355.

(6) Saenger, W. *Principles of Nucleic Acid Structure*; Cantor, C. R., Ed.; Springer-Verlag: New York, 1984; p 143.

(7) (a) Ono, A.; Cao, S. Q.; Togashi, H.; Tashiro, M.; Fujimoto, T.; Machinami, T.; Oda, S.; Miyake, Y.; Okamoto, I.; Tanaka, Y. *Chem. Commun.* **2008**, *39*, 4825. (b) Freeman, R.; Finder, T.; Willner, I. *Angew. Chem., Int. Ed.* **2009**, *48*, 7818. (c) Li, T.; Shi, L.; Wang, E.; Dong, S. *Chem. - Eur. J.* **2009**, *15*, 3347. (d) Wen, Y.; Xing, F.; He, S.; Song, S.; Wang, L.; Long, Y.; Li, D.; Fan, C. *Chem. Commun.* **2010**, *46*, 2596.

(8) (a) Miyake, Y.; Togashi, H.; Tashiro, M.; Yamaguchi, H.; Oda, S.; Kudo, M.; Tanaka, Y.; Kondo, Y.; Sawa, R.; Fujimoto, T.; Machinami, T.; Ono, A. *J. Am. Chem. Soc.* **2006**, *128*, 2172. (b) Tanaka, Y.; Oda, S.; Yamaguchi, H.; Kondo, Y.; Kojima, C.; Ono, A. *J. Am. Chem. Soc.* **2007**, *129*, 244. (c) He, S.; Li, D.; Zhu, C.; Song, S.; Wang, L.; Long, Y.; Fan, C. *Chem. Commun.* **2008**, 4885. (d) Liu, C. W.; Hsieh, Y. T.; Huang, C. C.; Chang, H. T. *Chem. Commun.* **2008**, 2242. (e) Deng, L.; Zhou, Z.; Li, J.; Li, T.; Dong, S. *Chem. Commun.* **2011**, *47*, 11065. (f) Lee, J. S.; Han, M. S.; Mirkin, C. A. *Angew. Chem., Int. Ed.* **2007**, *46*, 4093. (g) Xue, X.; Wang, F.; Liu, X. *J. Am. Chem. Soc.* **2008**, *130*, 3244. (h) Li, T.; Dong, S.; Wang, E. *Anal. Chem.* **2009**, *81*, 2144. (i) Zhu, Z.; Su, Y.; Li, J.; Li, D.; Zhang, J.; Song, S.; Zhao, Y.; Li, G.; Fan, C. *Anal. Chem.* **2009**, *81*, 7660.

(9) (a) Gellert, M.; Lipsett, M. N.; Davies, D. R. *Proc. Natl. Acad. Sci. U. S. A.* **1962**, *48*, 2013. (b) Simonsson, T. *Biol. Chem.* **2001**, *382*, 621. (c) Collie, G. W.; Parkinson, G. N. *Chem. Soc. Rev.* **2011**, *40*, 5867. (d) Sen, D.; Gilbert, W. *Nature* **1988**, *334*, 364. (e) Burge, S.; Parkinson, G. N.; Hazel, P.; Todd, A. K.; Neidle, S. *Nucleic Acids Res.* **2006**, *34*, 5402. (f) Davis, J. T.; Spada, G. P. *Chem. Soc. Rev.* **2007**, *36*, 296. (g) Golub, E.; Lu, C.-H.; Willner, I. *J. Porphyrins Phthalocyanines* **2015**, *19*, 65.

(10) (a) Wang, F.; Liu, X.; Willner, I. *Angew. Chem., Int. Ed.* **2015**, *54*, 1098. (b) Kang, H.; Liu, H.; Phillips, J. A.; Cao, Z.; Kim, Y.; Chen, Y.; Yang, Z.; Li, J.; Tan, W. *Nano Lett.* **2009**, *9*, 2690. (c) Dohno, C.; Uno, S. N.; Nakatani, K. *J. Am. Chem. Soc.* **2007**, *129*, 11898.

(11) (a) Osborne, S. E.; Matsumura, I.; Ellington, A. D. *Curr. Opin. Chem. Biol.* **1997**, *1*, 5. (b) Lee, J. F.; Stovall, G. M.; Ellington, A. D. *Curr. Opin. Chem. Biol.* **2006**, *10*, 282. (c) Willner, I.; Zayats, M. *Angew. Chem., Int. Ed.* **2007**, *46*, 6408. (d) Goulko, A. A.; Li, F.; Le, X. C. *TrAC, Trends Anal. Chem.* **2009**, *28*, 878. (e) Iliuk, A. B.; Hu, L.; Tao, W. A. *Anal. Chem.* **2011**, *83*, 4440. (f) Famulok, M.; Mayer, G. *Acc. Chem. Res.* **2011**, *44*, 1349. (g) Tuerk, C.; Gold, L. *Science* **1990**, *249*, 505. (h) Ellington, A. D.; Szostak, J. W. *Nature* **1990**, *346*, 818. (i) Robertson, M. P.; Ellington, A. D. *Nat. Biotechnol.* **2001**, *19*, 650.

(12) (a) Breaker, R. R.; Joyce, G. F. *Chem. Biol.* **1994**, *1*, 223. (b) Willner, I.; Shlyahovsky, B.; Zayats, M.; Willner, B. *Chem. Soc. Rev.* **2008**, *37*, 1153. (c) Famulok, M.; Hartig, J. S.; Mayer, G. *Chem. Rev.* **2007**, *107*, 3715. (d) Silverman, S. K. *Chem. Commun.* **2008**, 3467. (e) Joyce, G. F. *Annu. Rev. Biochem.* **2004**, *73*, 791. (f) Joyce, G. F. *Angew. Chem., Int. Ed.* **2007**, *46*, 6420.

(13) Aizen, R.; Golub, E.; Trifonov, A.; Shimron, S.; Niazov-Elkan, A.; Willner, I. *Small* **2015**, *11*, 3654.

(14) (a) Li, T.; Dong, S.; Wang, E. *J. Am. Chem. Soc.* **2010**, *132*, 13156. (b) Liu, D.; Balasubramanian, S. *Angew. Chem., Int. Ed.* **2003**, *42*, 5734. (c) Yang, Y.; Liu, G.; Liu, H.; Li, D.; Fan, C.; Liu, D. *Nano Lett.* **2010**, *10*, 1393.

(15) (a) Genot, A. J.; Bath, J.; Turberfield, A. J. *J. Am. Chem. Soc.* **2011**, *133*, 20080. (b) Zhou, M.; Dong, S. *Acc. Chem. Res.* **2011**, *44*, 1232. (c) Wang, L.; Zhu, J.; Han, L.; Jin, L.; Zhu, C.; Wang, E.; Dong, S. *ACS Nano* **2012**, *6*, 6659. (d) Pei, H.; Liang, L.; Yao, G.; Li, J.; Huang, Q.; Fan, C. *Angew. Chem., Int. Ed.* **2012**, *51*, 9020.

(16) (a) Shlyahovsky, B.; Li, Y.; Lioubashevski, O.; Elbaz, J.; Willner, I. *ACS Nano* **2009**, *3*, 1831. (b) Orbach, R.; Remacle, F.; Levine, R. D.; Willner, I. *Proc. Natl. Acad. Sci. U. S. A.* **2012**, *109*, 21228. (c) Stojanovic, M. N.; Stefanovic, D. *Nat. Biotechnol.* **2003**, *21*, 1069. (d) Li, T.; Ackermann, D.; Hall, A. M.; Famulok, M. *J. Am. Chem. Soc.* **2012**, *134*, 3508. (e) Orbach, R.; Willner, B.; Willner, I. *Chem. Commun.* **2015**, *51*, 4144.

(17) (a) Andersen, E. S.; Dong, M.; Nielsen, M. M.; Jahn, K.; Subramani, R.; Mamdouh, W.; Golas, M. M.; Sander, B.; Stark, H.; Oliveira, C. L. P.; Pedersen, J. S.; Birkedal, V.; Besenbacher, F.; Gothelf, K. V.; Kjems, J. *Nature* **2009**, *459*, 73. (b) Yang, Y.; Endo, M.; Hidaka, K.; Sugiyama, H. *J. Am. Chem. Soc.* **2012**, *134*, 20645. (c) Jester, S.-S.; Famulok, M. *Acc. Chem. Res.* **2014**, *47*, 1700. (d) Liu, X.; Lu, C.-H.; Willner, I. *Acc. Chem. Res.* **2014**, *47*, 1673.

(18) (a) Dittmer, W. U.; Reuter, A.; Simmel, F. C. *Angew. Chem., Int. Ed.* **2004**, *43*, 3550. (b) Krishnan, Y.; Simmel, F. C. *Angew. Chem., Int. Ed.* **2011**, *50*, 3124. (c) Bath, J.; Turberfield, A. J. *Nat. Nanotechnol.* **2007**, *2*, 275. (d) Goodman, R. P.; Heilemann, M.; Doose, S.; Erben, C. M.; Kapanidis, A. N.; Turberfield, A. J. *Nat. Nanotechnol.* **2008**, *3*, 93. (e) Teller, C.; Willner, I. *Curr. Opin. Biotechnol.* **2010**, *21*, 376. (f) Beissenhirtz, M. K.; Willner, I. *Org. Biomol. Chem.* **2006**, *4*, 3392. (g) Wang, F.; Willner, B.; Willner, I. *Top. Curr. Chem.* **2014**, *354*, 279.

(19) (a) Elbaz, J.; Wang, F.; Remacle, F.; Willner, I. *Nano Lett.* **2012**, *12*, 6049. (b) Elbaz, J.; Lioubashevski, O.; Wang, F.; Remacle, F.; Levine, R. D.; Willner, I. *Nat. Nanotechnol.* **2010**, *5*, 417. (c) Lu, C.-H.; Wang, F.; Willner, I. *J. Am. Chem. Soc.* **2012**, *134*, 10651.

(20) (a) Hudson, B.; Vinograd, J. *Nature* **1967**, *216*, 647. (b) Liu, L. F.; Perkocha, L.; Calendar, R.; Wang, J. C. *Proc. Natl. Acad. Sci. U. S. A.* **1981**, *78*, 5498. (c) Ryan, K. A.; Shapiro, T. A.; Rauch, C. A.; Griffith, J. D.; Englund, P. T. *Proc. Natl. Acad. Sci. U. S. A.* **1988**, *85*, 5844. (d) Trigueros, S.; Arsuaga, J.; Vazquez, M. E.; Sumners, D. W.; Roca, J. *Nucleic Acids Res.* **2001**, *29*, e67. (e) Dean, F. B.; Stasiak, A.; Koller, T.; Cozzarelli, N. R. *J. Biol. Chem.* **1985**, *260*, 4975.

DOI: 10.1021/jacs.6b00694
J. Am. Chem. Soc. 2016, 138, 5172–5185

(21) (a) Mao, C.; Sun, W.; Seeman, N. C. *Nature* **1997**, *386*, 137. (b) Du, S. M.; Stollar, B. D.; Seeman, N. C. *J. Am. Chem. Soc.* **1995**, *117*, 1194.
(22) Billen, L. P.; Li, Y. *Bioorg. Chem.* **2004**, *32*, 582.
(23) (a) Elbaz, J.; Wang, Z.-G.; Wang, F.; Willner, I. *Angew. Chem., Int. Ed.* **2012**, *51*, 2349. (b) Wu, Z.-S.; Shen, Z.; Tram, K.; Li, Y. *Nat. Commun.* **2014**, *5*, 4279.
(24) Sannohe, Y.; Sugiyama, H. *Bioorg. Med. Chem.* **2012**, *20*, 2030.
(25) Liu, Y.; Kuzuya, A.; Sha, R.; Guillaume, J.; Wang, R.; Canary, J. W.; Seeman, N. C. *J. Am. Chem. Soc.* **2008**, *130*, 10882.
(26) Schmidt, T. L.; Heckel, A. *Nano Lett.* **2011**, *11*, 1739.
(27) Lohmann, F.; Valero, J.; Famulok, M. *Chem. Commun.* **2014**, *50*, 6091.
(28) Lu, C.-H.; Cecconello, A.; Elbaz, J.; Credi, A.; Willner, I. *Nano Lett.* **2013**, *13*, 2303.
(29) Qi, X.-J.; Lu, C.-H.; Cecconello, A.; Yang, H.-H.; Willner, I. *Chem. Commun.* **2014**, *50*, 4717.
(30) Qi, X.-J.; Lu, C.-H.; Liu, X.; Shimron, S.; Yang, H.-H.; Willner, I. *Nano Lett.* **2013**, *13*, 4920.
(31) (a) Edblom, E. C.; Orban, M.; Epstein, I. R.J. *J. Am. Chem. Soc.* **1986**, *108*, 2826. (b) Rabai, G.; Beck, M. T. *J. Phys. Chem.* **1988**, *92*, 4831. (c) Rabai, G.; Orban, M.; Epstein, I. R. *Acc. Chem. Res.* **1990**, *23*, 258. (d) Rabai, G.; Epstein, I. R. *J. Am. Chem. Soc.* **1992**, *114*, 1529. (e) Lagzi, I.; Kowalczyk, B.; Wang, D.; Grzybowski, B. A. *Angew. Chem., Int. Ed.* **2010**, *49*, 8616. (f) Poros, E.; Horvath, V.; Kurin-Csorgei, K.; Epstein, I. R.; Orban, M. *J. Am. Chem. Soc.* **2011**, *133*, 7174.
(32) Hu, L.; Lu, C.-H.; Willner, I. *Nano Lett.* **2015**, *15*, 2099.
(33) Elbaz, J.; Cecconello, A.; Fan, Z.; Govorov, A. O.; Willner, I. *Nat. Commun.* **2013**, *4*, 2000.
(34) Shimron, S.; Cecconello, A.; Lu, C.-H.; Willner, I. *Nano Lett.* **2013**, *13*, 3791.
(35) Li, T.; Lohmann, F.; Famulok, M. *Nat. Commun.* **2014**, *5*, 4940.
(36) Lu, C.-H.; Qi, X.-J.; Cecconello, A.; Jester, S.-S.; Famulok, M.; Willner, I. *Angew. Chem., Int. Ed.* **2014**, *53*, 7499.
(37) Lu, C.-H.; Cecconello, A.; Qi, X. J.; Wu, N.; Jester, S.-S.; Famulok, M.; Matthies, M.; Schmidt, T.-L.; Willner, I. *Nano Lett.* **2015**, *15*, 7133.
(38) (a) Griffiths, K. E.; Stoddart, J. F. *Pure Appl. Chem.* **2008**, *80*, 485. (b) Dichtel, W. R.; Miljanic, O. S.; Spruell, J. M.; Heath, J. R.; Stoddart, J. F. *J. Am. Chem. Soc.* **2006**, *128*, 10388.
(39) (a) Campbell, C. J.; Leigh, D. A.; Vitorica-Yrezabal, I. J.; Woltering, S. L. *Angew. Chem., Int. Ed.* **2014**, *53*, 13771. (b) Beves, J. E.; Blight, B. A.; Campbell, C. J.; Leigh, D. A.; McBurney, R. T. *Angew. Chem., Int. Ed.* **2011**, *50*, 9260.
(40) Lee, C.-F.; Leigh, D. A.; Pritchard, R. G.; Schultz, D.; Teat, S. J.; Timco, G. A.; Winpenny, R. E. P. *Nature* **2009**, *458*, 314.
(41) Meng, Z.; Xiang, J.-F.; Chen, C.-F. *Chem. Sci.* **2014**, *5*, 1520.
(42) (a) Garaudée, S.; Silvi, S.; Venturi, M.; Credi, A.; Flood, A. H.; Stoddart, J. F. *ChemPhysChem* **2005**, *6*, 2145. (b) Raiteri, P.; Bussi, G.; Cucinotta, C. S.; Credi, A.; Stoddart, J. F.; Parrinello, M. *Angew. Chem., Int. Ed.* **2008**, *47*, 3536. (c) Ye, T.; Kumar, A. S.; Saha, S.; Takami, T.; Huang, T. J.; Stoddart, J. F.; Weiss, P. S. *ACS Nano* **2010**, *4*, 3697. (d) Jia, C.; Li, H.; Jiang, J.; Wang, J.; Chen, H.; Cao, D.; Stoddart, J. F.; Guo, X. *Adv. Mater.* **2013**, *25*, 6752. (e) Willner, I.; Pardo-Yissar, V.; Katz, E.; Ranjit, K. T. J. *Electroanal. Chem.* **2001**, *497*, 172. (f) Katz, E.; Lioubashevsky, O.; Willner, I. J. *J. Am. Chem. Soc.* **2004**, *126*, 15520.
(43) (a) Raymo, F. M.; Stoddart, J. F. *Chem. Rev.* **1999**, *99*, 1643. (b) Durola, F.; Heitz, V.; Reviriego, F.; Roche, C.; Sauvage, J.-P.; Sour, A.; Trolez, Y. *Acc. Chem. Res.* **2014**, *47*, 633. (c) Collin, J.-P.; Dietrich-Buchecker, C.; Gavina, P.; Jimenez-Molero, M. C.; Sauvage, J.-P. *Acc. Chem. Res.* **2001**, *34*, 477.
(44) Ackermann, D.; Schmidt, T. L.; Hannam, J. S.; Purohit, C. S.; Heckel, A.; Famulok, M. *Nat. Nanotechnol.* **2010**, *5*, 436.
(45) Ackermann, D.; Jester, S.-S.; Famulok, M. *Angew. Chem., Int. Ed.* **2012**, *51*, 6771.
(46) Lohmann, F.; Ackermann, D.; Famulok, M. *J. Am. Chem. Soc.* **2012**, *134*, 11884.
(47) Lohmann, F.; Weigandt, J.; Valero, J.; Famulok, M. *Angew. Chem., Int. Ed.* **2014**, *53*, 10372.
(48) Cecconello, A.; Lu, C.-H.; Elbaz, J.; Willner, I. *Nano Lett.* **2013**, *13*, 6275.
(49) Weizmann, Y.; Braunschweig, A. B.; Wilner, O. I.; Cheglakov, Z.; Willner, I. *Proc. Natl. Acad. Sci. U. S. A.* **2008**, *105*, 5289.
(50) Clarke, J.; Wu, H.-C.; Jayasinghe, L.; Patel, A.; Reid, S.; Bayley, H. *Nat. Nanotechnol.* **2009**, *4*, 265.
(51) (a) Wang, Z.-G.; Elbaz, J.; Remacle, F.; Levine, R. D.; Willner, I. *Proc. Natl. Acad. Sci. U. S. A.* **2010**, *107*, 21996. (b) Benenson, Y.; Adar, R.; Paz-Elizur, T.; Livneh, Z.; Shapiro, E. *Proc. Natl. Acad. Sci. U. S. A.* **2003**, *100*, 2191.
(52) Orbach, R.; Lilienthal, S.; Klein, M.; Levine, R. D.; Remacle, F.; Willner, I. *Chem. Sci.* **2015**, *6*, 1288.
(53) (a) Katz, E.; Sheeney-Haj-Ichia, L.; Willner, I. *Angew. Chem., Int. Ed.* **2004**, *43*, 3292. (b) Willner, B.; Katz, E.; Willner, I. *Curr. Opin. Biotechnol.* **2006**, *17*, 589.
(54) (a) Wang, F.; Liu, X.; Willner, I. *Adv. Mater.* **2013**, *25*, 349. (b) Tel-Vered, R.; Willner, I. *ChemElectroChem* **2014**, *1*, 1778.
(55) (a) Yildiz, H. B.; Tel-Vered, R.; Willner, I. *Angew. Chem., Int. Ed.* **2008**, *47*, 6629. (b) Tel-Vered, R.; Yehezkeli, O.; Yildiz, H. B.; Wilner, O. I.; Willner, I. *Angew. Chem., Int. Ed.* **2008**, *47*, 8272.
(56) Weigandt, J.; Chang, C. L.; Jester, S.-S.; Famulok, M. *Angew. Chem. Int. Ed.* **2016**, DOI: 10.1002/anie.201601042.
(57) Valero, J.; Lohmann, F.; Keppner, D.; Famulok, M. *ChemBioChem* **2016**, DOI: 10.1002/cbic.201500685.

NOTE ADDED IN PROOF

Within the process of publication of this perspective, two additional important papers describing the synthesis of daisy chain rotaxanes[56] and of a reconfigurable rotaxane[57] were reported.

DOI: 10.1021/jacs.6b00694
J. Am. Chem. Soc. 2016, 138, 5172−5185